November 2023

Elucidating the Priming Mechanism of ClpXP Protease by Single-Domain Response Regulator CpdR in Caulobacter crescentus

Kimberly E. Barker
University of Massachusetts Amherst

Elucidating the Priming Mechanism of ClpXP Protease by Single-Domain Response Regulator CpdR in *Caulobacter crescentus*

A Thesis Presented

by

KIMBERLY E. BARKER

Submitted to the Graduate School of the

University of Massachusetts Amherst in partial fulfillment

of the requirements for the degree of

MASTER OF SCIENCE

September 2023

Molecular and Cellular Biology

ELUCIDATING THE PRIMING MECHANISM OF CLPXP PROTEASE BY SINGLE-DOMAIN RESPONSE REGULATOR CPDR IN *CAULOBACTER CRESCENTUS*

A Thesis Presented

by

KIMBERLY E. BARKER

Approved as to style and content by:

DocuSigned by:
Peter Chien
250063B01A2348C...
Peter Chien, Chair

DocuSigned by:
Scott Garman
2744C3757EE2444...
Scott Garman, Member

DocuSigned by:
Margaret Stratton
02D707678942490...
Margaret Stratton, Member

DocuSigned by:
Margaret Stratton
02D707678942490...
Margaret Stratton, Department Head

Molecular and Cellular Biology

ACKNOWLEDGEMENTS

I would like to thank all the members of the Chien lab, my thesis committee, and my advisor Peter Chien for their continued guidance and support throughout the duration of my Master' thesis project. Specifically, I would like to thank my advisor Dr.Peter Chien, who helped guide me through my project and helped me understand how to approach scientific questions in an unbiased, discovery-based manner. He also showed me that science can be fun, and to search for discovery even in the most obscure places. I would like to thank Justyne Ogdahl, as she helped mentor me through learning biochemical assays and chromatography principles as an undergraduate researcher, which helped me to lay down the basis of my thesis work. I also want to thank the entire Chien lab for providing a fun, collaborative work environment, and I will miss our Worcester/Blue Wall lunch outings. Last but definitely not least, I want to thank my family and friends for being my support system throughout my time at UMass. I could not have completed this process without the emotional support from my own personal cheerleading team. Specifically, thank you to my loving partner Alex, who listened to me when I was down, and pushed me to continue through failures and hard days. I could not have completed this work without my amazing support system, both in the lab and at home.

ABSTRACT

ELUCIDATING THE PRIMING MECHANISM OF CLPXP PROTEASE BY SINGLE-DOMAIN RESPONSE REGULATOR CPDR IN *CAULOBACTER CRESCENTUS*

SEPTEMBER 2023

KIMBERLY E. BARKER, B.S., UNIVERSITY OF MASSACHUSETTS AMHERST

M.S., UNIVERSITY OF MASSACHUSETTS AMHERST

Directed by: Professor Peter Chien

In *Caulobacter crescentus*, progression through the cell cycle is regulated by the AAA+ protease ClpXP, and there are several classes of cell-cycle substrates that require adaptors in order to be degraded. CpdR, a single domain-response regulator, binds the N-terminal domain of ClpXP and primes the protease for degradation of downstream factors (Lau et al., 2015). The ability of CpdR to bind ClpX is regulated by its phosphorylation state. In the unphosphorylated state, CpdR binds ClpXP and guides its localization to the cell pole during the swarmer to stalked transition, where CpdR is mediates degradation of substrates such as PdeA. Phosphorylation of response regulator receiver domains requires magnesium as a cofactor to stabilize the phosphorylated aspartate and reciprocally, phosphorylated receiver domains bind magnesium more effectively. While it is understood that CpdR primers ClpX for substrate degradation, the mechanism by which it does so has remained unclear. Using CollabFold, we identified putative residues involved in CpdR-ClpX binding and validated them using a BACTH screening. In vitro, we characterized the role that magnesium plays in regulating CpdR binding to ClpX. In this work, we directly test the role of magnesium in CpdR priming of ClpXP to show that magnesium may play a regulatory role in CpdR-mediated degradation, and thus binding to ClpX. We identify residues in ClpX that seem to be important for CpdR binding, which prior to this work was not clear.

TABLE OF CONTENTS

Page

LIST OF TABLES

Table Page

LIST OF FIGURES

Figure Page

CHAPTER 1

INTRODUCTION

1.1. AAA+ Proteases and Cell Cycle Dependent Proteolysis

In both eukaryotes and prokaryotes, the cell cycle depends on the tight regulation of protein synthesis and degradation. Maintaining the balance of proteins is critical to ensure cell survival and avoid toxic overexpression. Thus, proteases in the cell must demonstrate a certain level of substrate specificity. In eukaryotes, proteome homeostasis is maintained by two main pathways, including the ubiquitin proteasome pathway and lysosomal proteolysis. In the ubiquitin proteasome pathway, proteins are covalently tagged with ubiquitin in a multistep process by which ubiquitin is transferred from E1 enzyme to the enzyme E2 and finally E3 ubiquitin ligase, which transfers ubiquitin to a target protein allowing degradation by the proteasome (Cooper GM, 2000). In lysosomal proteolysis, proteins are up taken by the lysosome, for example by autophagy, where enzymes in the lysosome ultimately degrade the proteins. In bacteria, ATPases associated with various cellular activities (AAA+) recognize substrates and harvest energy via ATP hydrolysis to unfold, translocate, and degrade substrates. There are various AAA+ proteases that are highly conserved in bacteria, including ClpXP, ClpAP, and Lon (Sauer and Baker, 2012). ClpXP and ClpAP have separate unfoldase subunits and peptidase subunits, while the Lon protease contains an unfoldase and peptidase domain encoded on the same polypeptide (Olivares et al., 2016). In *Caulobacter crescentus,* progression through the cell cycle is regulated by the AAA+ protease ClpXP, where mobile swarmer cells must transition to a non-mobile stalked cell in order to replicate (Jenal, 2009). The swarmer to stalked cell transition, which is analogous to the G1-S phase in Eukaryotes, is regulated by both the synthesis and degradation of specific proteins at certain phases of the cell cycle.

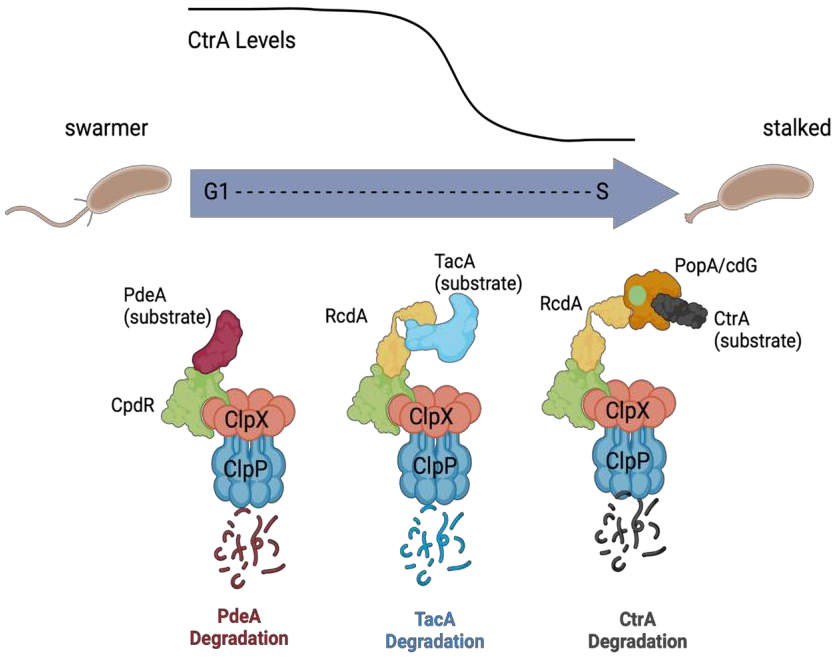

Figure 1-1. An Adaptor Hierarchy Regulates Substrate Specificity in Caulobacter Crescentus (Adapted from Joshi et al., 2015).

While ClpXP is capable of degrading some targets without assistance, adaptor proteins help to increase substrate specificity and increase the volume of the protease substrate pool (Mahmoud and Chien, 2018). Because ClpX and ClpP levels remain constant throughout the cell cycle, the adaptor proteins are critical in regulating protein homeostasis. There are several classes of cell-cycle substrates that require various adaptors in order to be degraded by ClpXP (Figure 1). Previous studies have shown that the protein CpdR, a single domain-response regulator, binds the N-terminal domain of ClpXP and primes the protease for degradation of downstream factors (Lau et al., 2015). CpdR is critical for enhancing substrate degradation. *In vitro*, two other adaptors RcdA and PopA are required for degradation of CtrA and other substrates as well. RcdA only binds the stalk synthesis transcription factor TacA in addition to ClpXP after protease priming by CpdR (Joshi et al., 2015). This adaptor hierarchy regulates the swarmer-to-stalked transition in

Caulobacter crescentus, and CpdR is a key adaptor that primes downstream selective protein degradation.

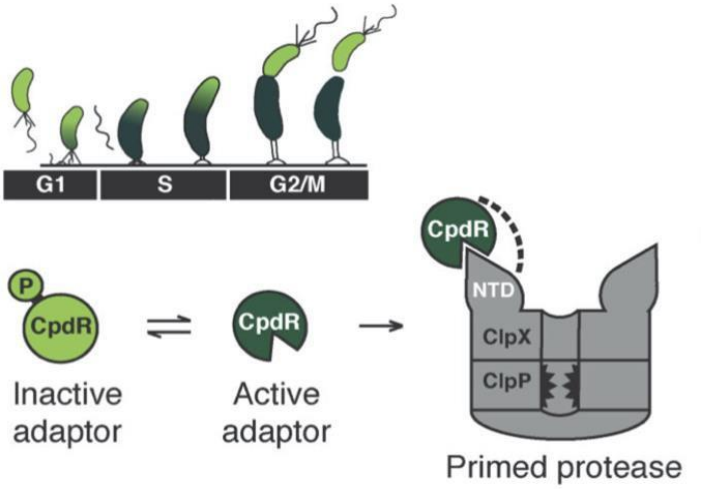

Figure 1-2. Phosphorylation Regulates Single-Domain Response Regulator CpdR (Lau et al. 2015)

The ability of CpdR to bind ClpX is regulated by its phosphorylation state. In the unphosphorylated state, CpdR binds ClpXP and guides its localization to the cell pole during the swarmer to stacked transition. Upon phosphorylation of CpdR, ClpXP is observed to delocalize from the cell pole, and the transcription factor CtrA is not degraded (Figure 1-2). Both CpdR and CtrA are regulated by CckA histidine kinase. Phosphorylation of CtrA creates an active CtrA, while conversely phosphorylation of CpdR is inactivating (Figure 1-3). The phosphorylation of CpdR and CckA enables a redundant regulatory mechanism for CtrA degradation (Iniesta et al. 2006).

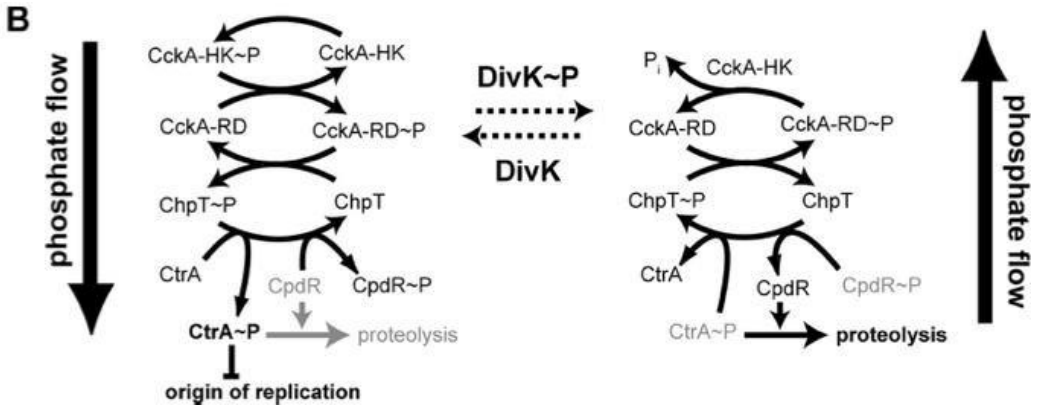

Figure 1-3. A Phospho-Relay System Enables Redundant Regulation of CtrA degradation in *Caulobacter Crescentus* (Chen et al. 2009).

1.2. Types of Adaptors and their Independent Mechanisms of Action.

Adaptors function to bring substrate in close proximity to their binding partner, however, the mechanism by which they do so can vary depending on the adaptor at hand. For example, an adaptor can merely act as a scaffold by binding one or more proteins to bring all components in close proximity to enable downstream signaling events. Scaffold proteins can act as a tether to increase the local concentration of binding partners and thus increase binding interactions, or they can enable an allosteric effect to regulate binding efficiency (Good et al. 2011). For example, the adaptor of ClpXP in *E. coli* SspB binds both ssrA-tagged substrates as well as ClpX, acting to bring both molecules in close proximity to each other, such that at high concentrations of SspB, there is an overall inhibitory effect on substrate binding. On the other hand, substrate recognition to ClpX is not limited at saturating concentrations of CpdR, indicating that CpdR does not function simply as a scaffold, rather that it acts to prime the protease into an active state (Figure 1-4). Binding of CpdR to ClpX alone is weak, however, the presence of adaptor, ClpX, and substrate results in an overall strong binding event that differs from other types of bacterial adaptors such as SspB (Lau et al. 2016). The difference in adaptor mechanism between CpdR and SspB allows CpdR the advantage to prevent inhibition at high adaptor concentration.

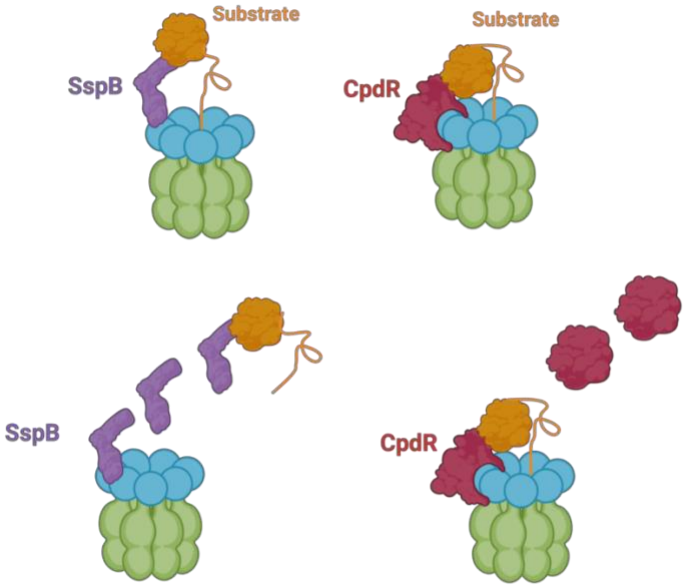

Figure 1-4. Scaffolding adaptors show limitations at high concentrations (adapted from Lau et al. 2016).

1.3. Conservation Amongst Single-Domain Response Regulators

1.3.1. Receiver Domain Structure and Function in Response Regulators

Response regulator proteins are characterized by their receiver domains, which act to regulate function via phosphorylation-mediated activation. Phosphorylation of the receiver domains in response regulators translates to structural changes in the signaling output face (Bourret et al., 2010). CpdR contains a conserved structure shared amongst single-domain response regulator receiver domains. Specifically, receiver domains contain a $(\beta\alpha)_5$ structure (Figure 1-4). Within the three central beta-strands in receiver domains are conserved active sites. Specifically, there are three highly conserved aspartic acid residues that are important for coordinating metal ions, specifically magnesium. Additionally, β_3 ends in a conserved aspartic acid residue which acts as the site of phosphorylation. For CpdR, phosphorylation occurs at Asp 51, and magnesium ion coordination is performed at residues D9, D10, and D11. Other conserved residues important for

phosphorylation-mediated conformational changes include a highly conserved lysine at the end of β_5. The phosphorylation mediated conformational changes are primarily localized to the $\alpha_4\beta_5\alpha_5$ face of the receiver domain. These conserved residues amongst response regulators gives us a platform upon which to begin understanding CpdR structure and function.

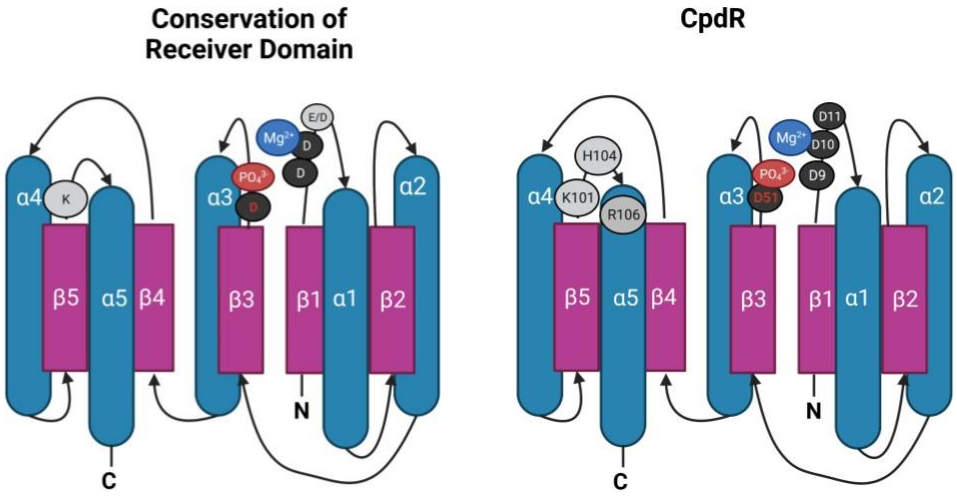

Figure 1-5. Conservation of Receiver Domains in Single-Domain Response Regulators.

1.3.2. CheY is a well-characterized Single-Domain Response Regulator

In bacteria, CheY is the best characterized single-domain response regulator. CheY acts to regulate bacterial chemotactic response, where it binds FliM resulting in a change in flagellar rotation (Solà et al. 2000). Magnesium-bound CheY can be phosphorylated to transition the protein to an active conformation. Previous work has shown that for CheY, reducing the negative charge within the active site either by mutations or introducing a positive magnesium cation increased the stability of CheY (Figure 1-6). Additionally, Asp 13 and Asp 13 in CheY are involved in Mg^{2+} coordination (Bellsolell et

al. 1994). Understanding and comparing conserved structural components of the well-characterized CheY to CpdR can help us to understand the structure and function of specific residues within CpdR.

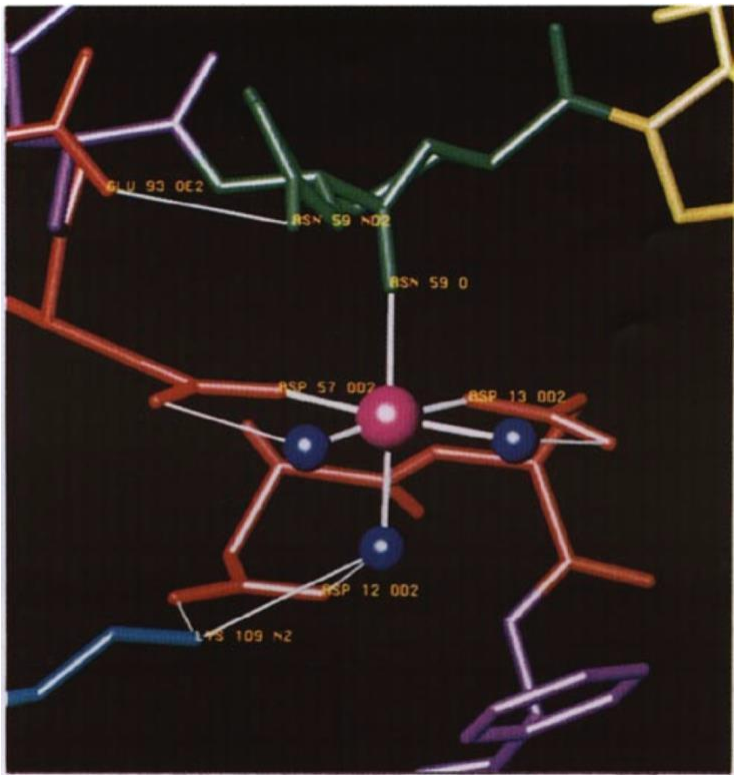

Figure 1-6. Magnesium Coordination by CheY is required for phosphorylation and increases protein stability (Bellsolell et al. 1994).

1.3.3. Mutants in CpdR Conserved Signaling Output Face Impact CpdR-Mediated Degradation

It is understood that phosphorylation of response regulators translates to conformational changes in the signaling output face that impact adaptor function. Previous work has shown that mutations within the predicted signaling output of CpdR results in a deficiency in substrate degradation of CpdR-dependent substrates. Specifically, mutating residues H104 and R106 to alanine resulted in

defective degradation of substrate PdeA (Figure 1-7). While R106A was able to achieve wild-type activity at saturating adaptor concentrations, the H104A mutant was unable to do so. Due to their respective importance in mediating substrate degradation, it has been postulated that these residues may be at or near the binding interface for ClpX.

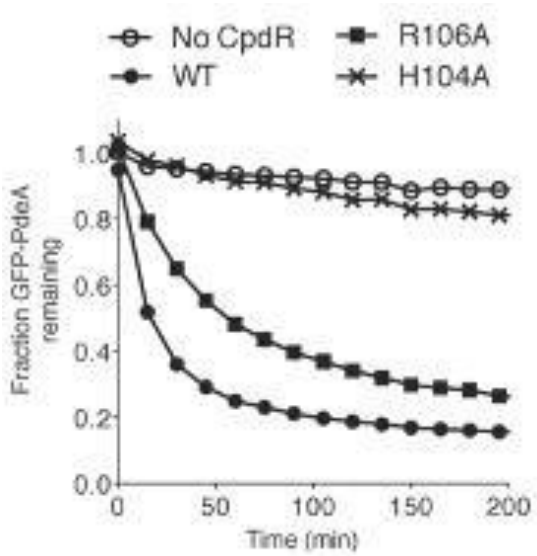

Figure 1-7. Mutations in Signaling Output Face of CpdR fail to efficiently deliver substrate (Joanne Lau dissertation, 2016)

In addition to identifying mutants that fail to deliver substrate, previous work has identified mutants of CpdR that improve substrate delivery and binding. Through a suppressor screen to identify mutants of CpdR that recover the H104A phenotype, a mutation D9G was identified to recover both binding and substrate delivery of the H104A mutant (Figure 1-8). Because the D9 residue is involved in magnesium coordination in CpdR, it is thought that this mutant of CpdR binds magnesium less readily, which could result in a more active conformation of CpdR. Overall, the previously identified mutants provide a basis upon which to investigate the binding interface of CpdR and ClpX.

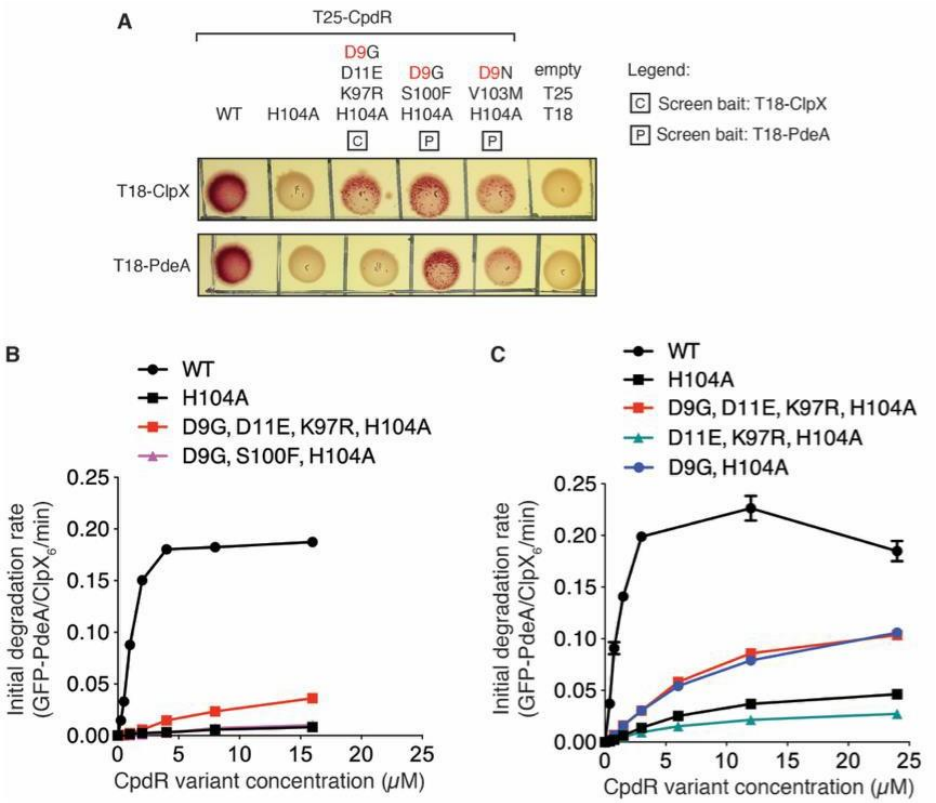

Figure 1-8. Identifying activating mutants of CpdR H104A via a suppressor screen (Joanne Lau dissertation, 2016).

1.3.4. Thesis structure

This thesis outlines work to understand how CpdR primes the ClpX protease in *C. Crescentus*. Chapter 1 provides a review of the current understand of CpdR function as an adaptor, and a review of the literature regarding single domain response regulators broadly. Chapter 2 highlights the project to uncover mutants of both CpdR and ClpX that show deficiency in binding using a site-directed mutagenesis approach based on AlphaFold2 predictions. Chapter 3 will uncover work to understand the role in which magnesium plays in regulating CpdR-dependent substrate delivery, and how magnesium plays a role in either promoting or inhibiting adaptor binding. Finally, chapter 3 will summarize the conclusions of each project, and the future directions that relate to the findings in this work.

CHAPTER 2

ELUCIDATING CLPX CPDR INTERACTION VIA SITE-DIRECTED MUTAGENESIS

2.1. Introduction: Identifying Putative CpdR-ClpX Binding Sites via AlphaFold2 Multimer

The first aim of my thesis project was to further elucidate the binding interface of CpdR and ClpX. While previous work has identified CpdR residues necessary for ClpX binding and substrate degradation, the specific binding interface has not been identified. Due to the limitations of purifying CpdR and ClpX to high concentrations, it has been difficult in the past to perform HDX-MS or other biophysical methods to identify residues involved in CpdR-ClpX binding. Thus, we sought to utilize predictive modeling to identify putative interactions between the two proteins. Using AlphaFold2 Multimer in CollabFold, we introduced duplicates of the sequence of CpdR, the N-terminal domain of ClpX, and RcdA, such that we could predict the binding interface of CpdR with the N-terminal domain (NTD) of ClpX. Since the ClpX NTD dimerized, entering duplicate sequences would help to identify more accurate binding sites that are not within the dimerization interface.

To give us confidence in our model, we first looked to see if the experimentally validated residues on CpdR that are known to be important for substrate degradation were facing toward the N-terminal domain of ClpX. Interestingly, we observed that the H104 residue was oriented towards the conserved cluster of cysteines in ClpX that are known to coordinate a zinc ion (Figure 2-1). ClpX contains a type C4 zinc binding domain (ZBD) housing 4 highly conserved cysteine residues that play a role in coordinating zinc. It has been shown that the ZBD of ClpX plays an essential role in function, and it is thought that ATP binding drives a conformational changed involving this domain (Donaldson et al. 2003).

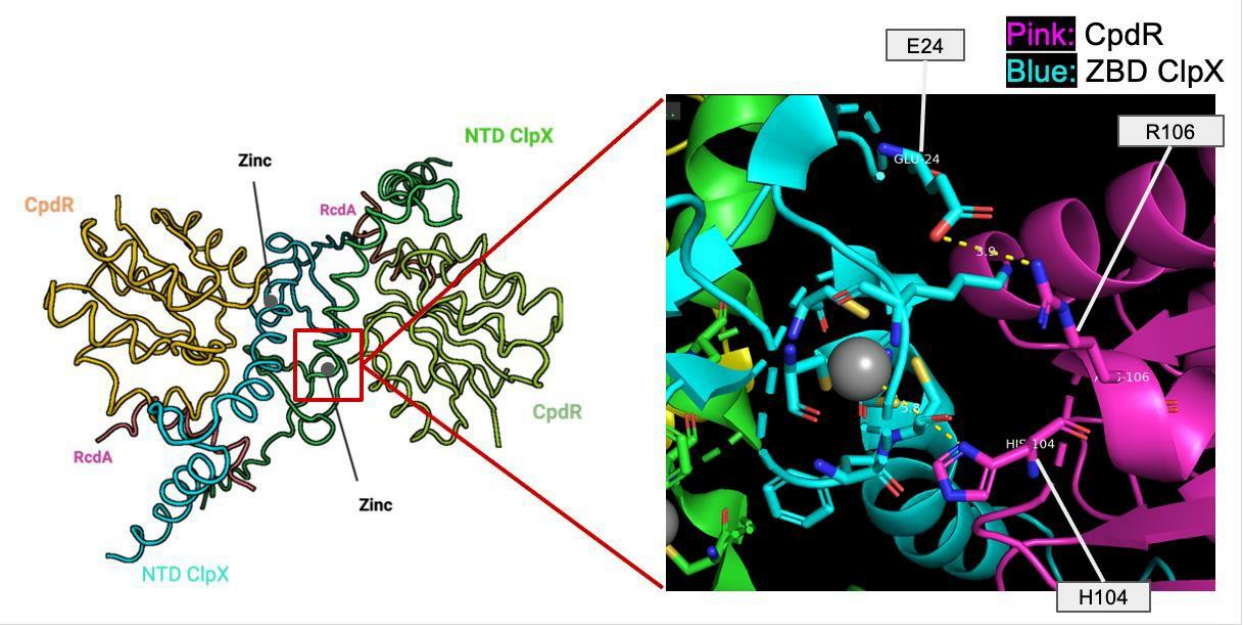

Figure 2-1. Identifying putative CpdR-ClpX binding interactions using CollabFold. Sequences of CpdR (accession A0A0H3C5J9), NTD ClpX (1-61 AA, accession B8GX14), and RcdA (accession A0A0H3CD07) were entered as input sequences to CollabFold (Mirdita, M., 2022). The model with the highest confidence (model 1, rank 1) was chosen for further analysis.

Beyond cysteine, there are several known amino acids that are chemically capable of coordinating metal ions including zinc. Depending on the type of site on a protein, certain residues are chemically predominant for coordination over others. Catalytic sites tend to favor histidine residues for coordination, while in structural sites cysteine residues dominate coordination. There have also been sites of zinc playing a role in quaternary structure, where zinc is bound within the binding interface of two proteins, characterized as a zinc binding protein inteface (DS Auld, 2001).

Because of the known role of the ZBD in regulating ClpX function, we became interested in the postulation that the H104 residue is not necessarily binding a specific residue on ClpX, rather, the histidine residue could possibly be coordinating the zinc within the cysteine cluster on ClpX, which in turn drives conformational changes that regulate function.

In addition to the H104 residue, we looked at the R106 residue orientation to give confidence in our model. Interestingly, the R106 residue was predicted to form a salt bridge with the E24 residue on ClpX within 3 angstroms of each other. Based on the observation of the H104 and R106 residues positioning toward the ClpX NTD, we wanted to look at other residues of CpdR and ClpX that could serve as potential binding interactions.

First, I looked at conserved residues within response regulators on CpdR to see if there were any interesting putative interactions with ClpX. I observed that the conserved lysine at the end of β_5 in CpdR was in close proximity to the aspartic acid residue D46 on ClpX. Given the conservation of this lysine and its known role in phosphorylation-mediate conformation changes, I was curious if this lysine may play a role in binding ClpX, especially due to its proximity to the H104 residue which has been experimentally shown to be important for binding.

Next, I looked at the conserved aspartic acid residues known to coordinate magnesium in phosphorylation, as magnesium binding and phosphorylation play a role in regulating CpdR activity and localization. The D9 residue of CpdR was observed to be in close proximity to K53 on ClpX, such that they could form a salt bridge. I thought this was interesting, as magnesium coordination at the D9 residue would block this salt bridge from occurring. Thus, when CpdR is phosphorylated and bound to magnesium, this salt bridge would be inhibited. However, when CpdR is mutated to D9G, there is a recovery of CpdR H104A binding. Thus, this predicted salt bridge provided an interesting possible explanation as to the importance of magnesium binding at this site and CpdR activity regulation.

Finally, I observed that a conserved serine on CpdR S12 was oriented toward residue D46 on ClpX, in such a way that they could hydrogen bond. While hydrogen bonding in predictive

software's is not typically something I would look into, I found this interesting as previous work of the ClpX ZBD showed through sequence conservation analysis that residue D46 was similar in >80% of the sequences from over 100 different bacteria aligned using ClustalW (Donaldson et al 2003). Due to the conservation of this residue in ClpX, I wanted to look into this interaction further to see if the S12 residue may be involved in ClpX binding.

In summary, I generated 5 mutants total to further validate the putative interactions based on the CollabFold prediction (Table 2-1). I screened mutants via a bacterial adenylyl cyclase two-hybrid (BACTH) approach which I then would validate *in vitro* upon a negative interaction in the screen.

Table 2-1. CpdR and ClpX Mutants to Validate Predicted Interactions.

CpdR Mutants	ClpX Mutants
S12A	E24K
K101A	K53E
H104E/C	

2.2. Validating CpdR Mutants via Bacterial Adenylyl Cyclase Two-Hybdrid Approach

After identifying putative binding residues using CollabFold, CpdR mutants were generated in a pKT25 vector using around-the-horn cloning. Upon validation of mutations by nanopore sequencing, I transformed either pKT25-WT CpdR, an empty pKT25 vector, or the respective mutant pKT25 CpdR vector into a bacterial two-hybrid chemically competent cells (BTH101) with a ΔClpX chromosomal knockout containing pUT18C WT ClpX to screen for negative interactions. Upon transformation, it was observed that mutating the H104 residue of CpdR to another residue capable of coordinating zinc failed to recover the binding phenotype of the H104A mutant. If the H104 residue was coordinating zinc at the ClpX NTD, we would have expected a recovery in binding when mutating to a cysteine or a glutamic acid. Additionally, the mutants K101A and S12A failed to show a reduction in binding as expected by the CollabFold predictions. Based on

the results of the BACTH assay, it appears that this portion of the prediction in CollabFold is not representative of the true binding interactions within CpdR and ClpX.

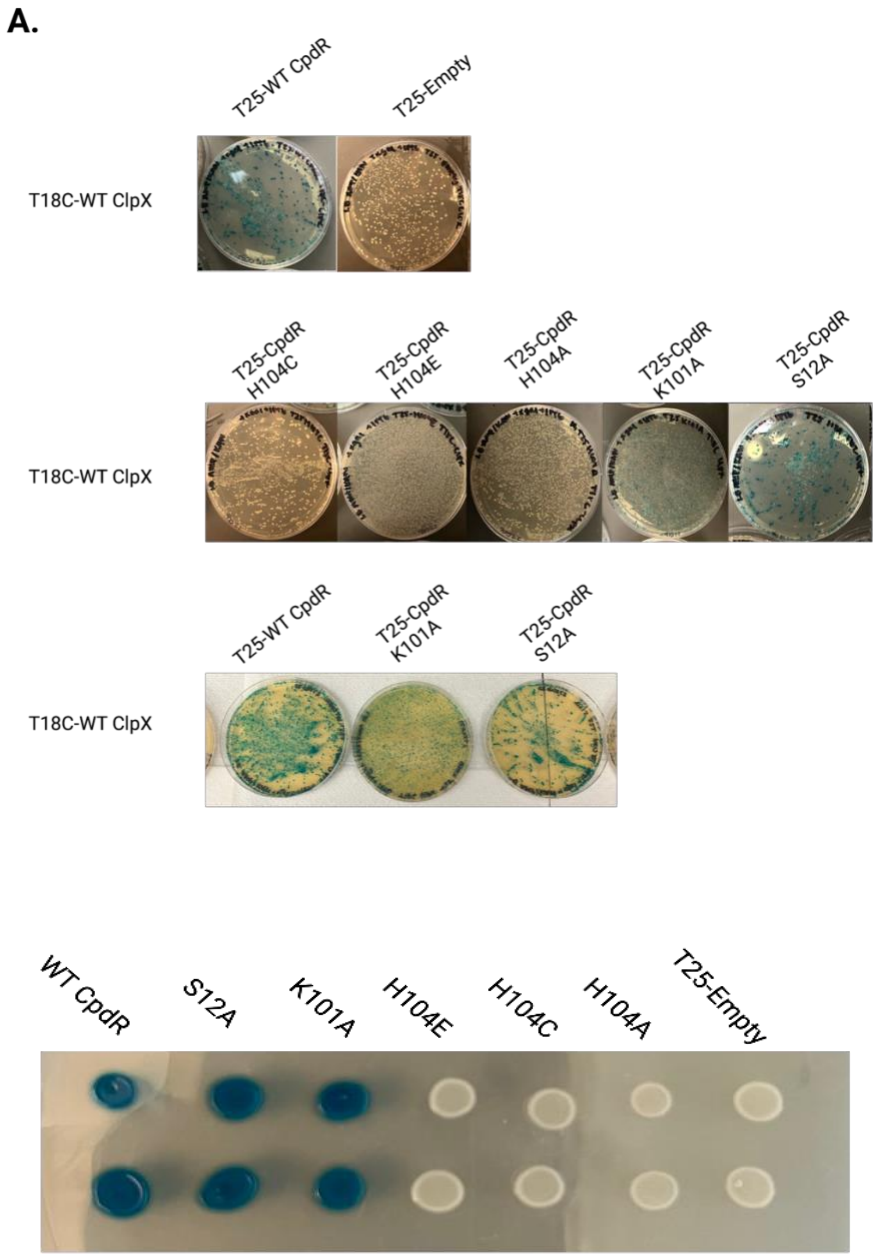

Figure 2-2. Screening CpdR Putative Mutants via Bacterial Adenylyl Cyclase Two-Hybrid Approach. A. ΔClpX BTH101 cells containing pUT18C-WT ClpX were transformed with pK25-WT CpdR, pK25-Empty, or pK25-Mutant CpdR. Transformations were plated on LB X-gal+IPTG on their respective antibiotic marker. Plates were allowed to incubate for 2-3 days.

(Figure 2-2 cont.) **B.** After 2-3 days of incubation, the respective plates were scraped fully to collect a representative population of each transformation, and resuspended in 200 uL sterile MilliQ water and plated on X-gal and IPTG to observe the population level expression of beta-galactosidase.

2.3. Validating ClpX Mutants via Bacterial Adenylyl Cyclase Two-Hybdrid Approach

After identifying putative binding residues using CollabFold, ClpX mutants were generated in a pUT18C vector using around-the-horn cloning. Upon validation of mutations by nanopore sequencing, I transformed either pUT18C-WT ClpX, An empty pUT18C vector, or the respective mutant pUT18C vector into a bacterial two-hybrid chemically competent cells (BTH101) with a ΔClpX chromosomal knockout containing WT CpdR to screen for negative interactions. Interestingly, upon transformation, it was observed that both the E24K and K53E showed reduced strength in binding as demonstrated by a reduction in the number of blue colonies present in both mutants (Figure 2-3A). When scraping the entire plate to gain a representation of the population expression, it was more clear that for both mutants, while there was still some interaction present as shown by the slight blue color in both mutants, there was a reduction in the strength of the blue saturation as compared to wild-type (Figure 2-3B). Based on both the ratio of blue to white colonies for each mutant and the saturation of blue coloration when scraping the whole plate and replating the sample, it appeared that both E24K and K53E show an intermediate level of binding to WT CpdR as compared to WT and empty vector.

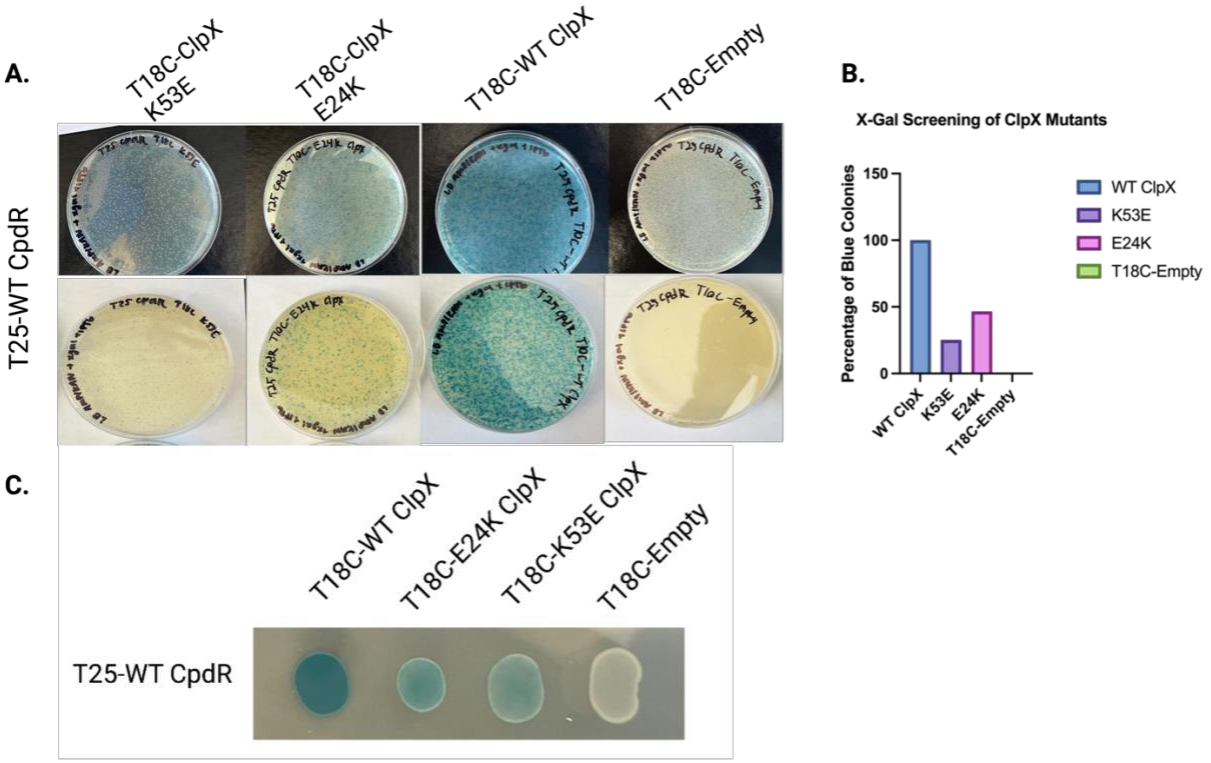

Figure 2-3. Screening CollabFold ClpX Mutants via Bacterial Adenylyl Cyclase Two-Hybrid Approach. A. ΔClpX BTH101 cells containing pKT25-WT CpdR were transformed with pUT18C-WT ClpX, pUT18C-Empty, or pUT18C-Mutant CpdR. Transformations were plated on LB X-gal+IPTG on their respective antibiotic marker. Plates were allowed to incubate for 2-3 days. **B.** After 2-3 days of incubation, the respective plates were scraped fully to collect a representative population of each transformation, and resuspended in 200 uL sterile MilliQ water and plated on X-gal and IPTG to observe the population level expression of beta-galactosidase.

However, to validate the data, I repeated the same transformation multiple times, and upon repetition, the K53E mutant appeared to look like wild-type ClpX in terms of blue coloration (Figure 2-4). Additionally, to validate that the E24 residue was specifically interacting with the R106 residue on CpdR, I created a charge swap of CpdR (R106E) to see if charge swapping both would recover binding in a BACTH system. Surprisingly, charge swapping both did not recover binding of E24K, and in fact made binding worse than E24K alone (Figure 2-4).

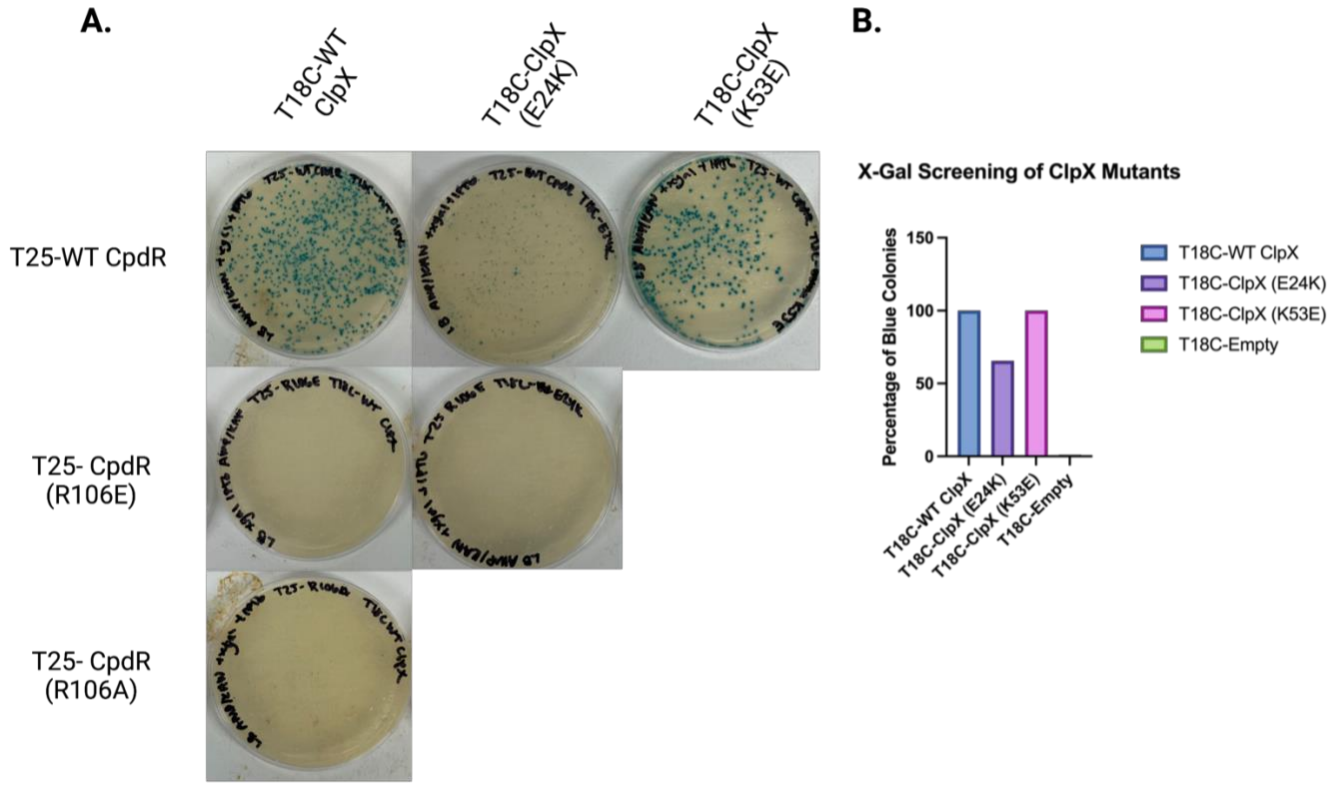

Figure 2-4. Validating initial BACTH results of ClpX Mutants. A. Repeating BACTH transformation in BTH101 cells was performed and cells were plated on LB Agar containing x-gal and IPTG to induce expression of respective vectors. Transformants were allowed to grow at 30^{o}C for 2-3 days, or until wild-type cells were fully blue. B. The ratio of blue colonies to white colonies was calculated by quantifying both blue and white colonies in a fixed area and calculating the ratio of blue colonies to the total number of colonies in that area. Colonies were quantified using ImageJ.

2.4. Characterizing ClpX mutant deficient in SspB mediated delivery in the context of CpdR as an adaptor.

CpdR and SspB both play independent roles in mediating substrate delivery for ClpX. While SspB is thought to be a scaffolding adaptor, CpdR is thought to act as a protease-priming adaptor where binding of protease, adaptor, and substrate is required to deliver substrate. While both SspB bind ClpX, it is not clear whether or not CpdR and SspB share a binding interface. Previous work with SspB and the ClpX NTD in *E. coli* used NMR analysis to identify residues in the ClpX NTD important for SspB binding. They observed that upon addition of SspB, the chemical shift of

residue A29 disappeared, indicating that this residue is at or near the binding interface with ClpX. Additionally, they claimed that upon mutation of A29 to A29N, there was an abolishment of the effect of SspB addition for degradation enhancement of GFP-SsrA

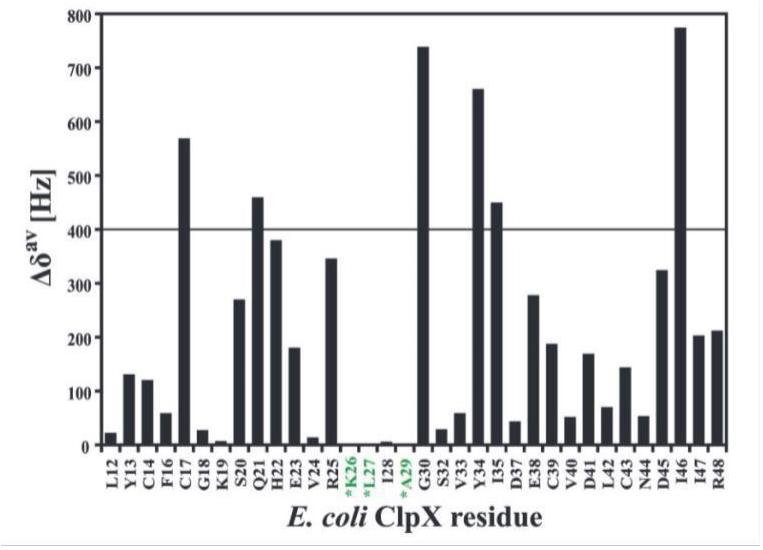

Figure 2-5. NMR Shifts of ClpX NTD in *Escherichia Coli* (Thibault et al. 2006).

To understand whether or not SspB and CpdR bind the same interface, I generated this A29N ClpX mutant in *C. Crescentus* and characterized the mutant for both SspB and CpdR *in vitro.*

First, I wanted to characterize SspB with A29N to ensure that the mutation showered a decrease in SspB mediated delivery. However, upon investigation, it was observed that while A29N ClpX showered overall reduced activity as compared to wild-type (Figure 2-4A), there was no difference in terms of fold-change of degradation rate upon addition of SspB (Figure 2-4B). To ensure the difference in activity between A29N and WT ClpX was not due to differences in concentration of active, hexameric ClpX, I executed an ATP titration to ensure the two proteins showed similar levels of ATP hydrolysis, indicating similar protein concentrations. Upon titration, both WT and A29N showed very similar ATPase rates at increasing concentrations of ATP, indicating the difference in activity was not due to concentration dependent effect of protease, rather, due to the mutation of the protease itself (Figure 2-4C). While the NMR data of *E. coli* ClpX seemed to

indicate that the A29 residue was at or near the binding interface for SspB, the degradation data for GFP-SsrA opposes this observation.

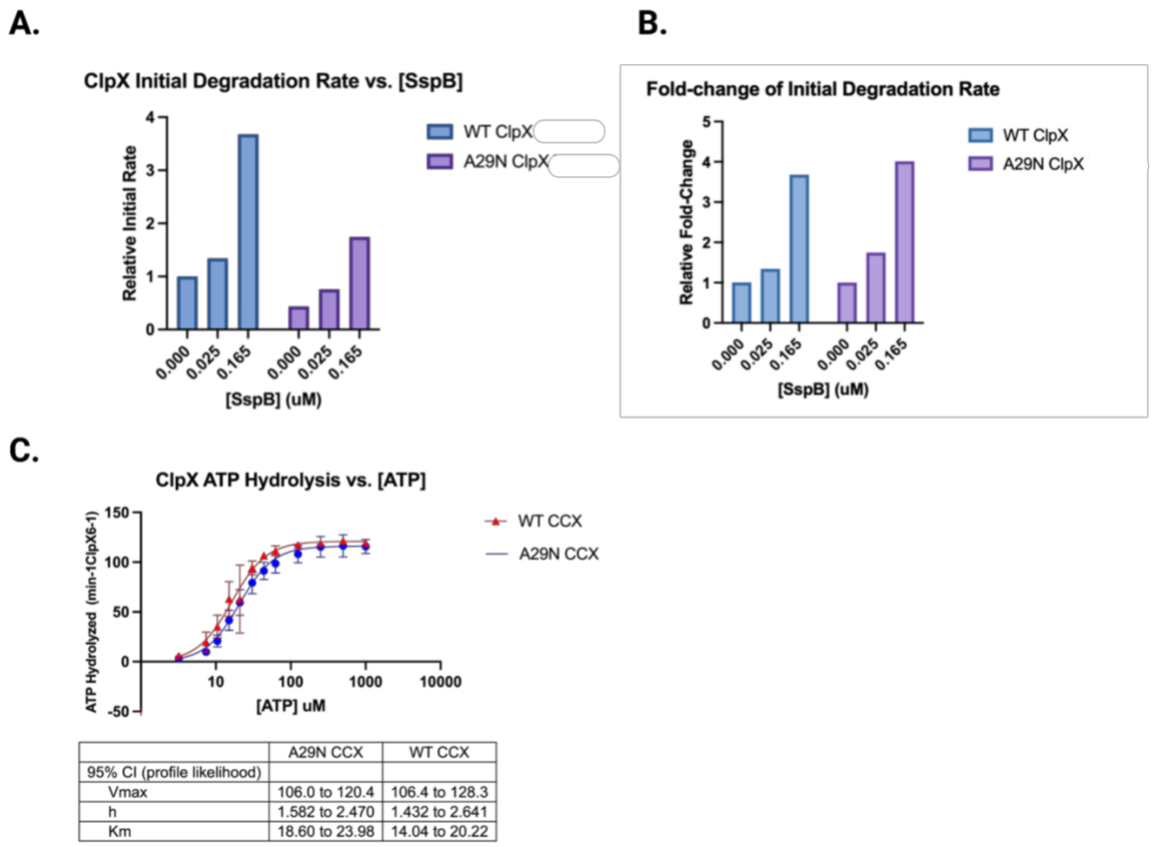

	A29N CCX	WT CCX
95% CI (profile likelihood)		
Vmax	106.0 to 120.4	106.4 to 128.3
h	1.582 to 2.470	1.432 to 2.641
Km	18.60 to 23.98	14.04 to 20.22

Figure 2-6. Characterizing ClpX A29N mutant *in vitro*. *A and B.* SspB was titrated at increasing concentrations and degradation of GFP-SsrA was monitored over 30 minutes. Concentrations of components included 0.16 uM ClpX (hexamer), 0.1 uM ClpP (tetradecamer), (Figure 2-5 cont.) and 1 uM substrate. C. ATP was titrated at increasing concentrations from 0 to 1 mM ATP. ATP was regenerated using an ATP regeneration mix. ATP consumption was monitored by an NADH coupled reaction. Protease concentration was calculated to 0.1 uM ClpX (hexamer) final.

Regardless of the lack of fold-change for SspB-mediated delivery, I then went on to characterize CpdR in the same context. Similar to SspB, there did not seem to be a difference in CpdR mediated degradation between the A29N mutant and WT CpdR (Figure 2-5). Since both SspB and CpdR do not seem to show differences in delivering substrate for both WT and A29N ClpX, it is not clear from these experiments whether or not CpdR and SspB share a binding interface.

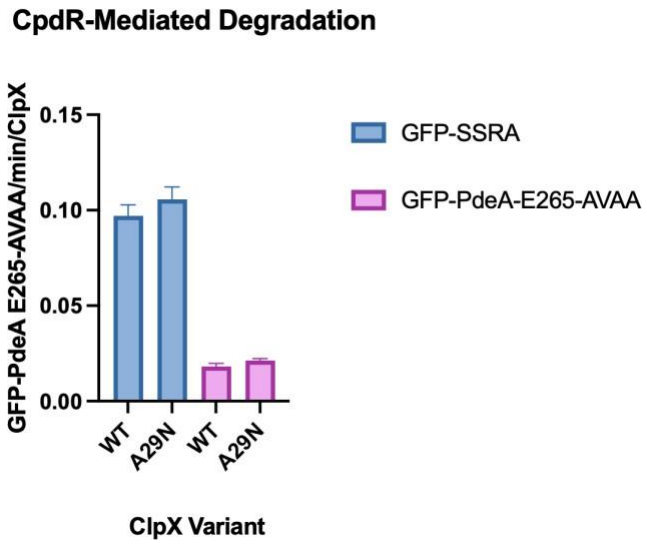

Figure 2-7. Characterizing ClpX A29N Mutant with CpdR *in vitro*. Substrate delivery of either GFP-SsrA or GFP-PdeA-E265-AVAA was monitored over the time frame of 30 min in the presence or absence of CpdR. Concentrations of components were as follows: 0.4 uM ClpX (hexamer), 0.8 uM ClpP (tetradecamer), 1 uM GTP, 2 uM CpdR, and 2 uM substrate.

2.5. Conclusions and Future Directions.

Using CollabFold to predict protein-protein interactions and BACTH as a method of screening for positive interactions, I was able to identify and validate putative mutations in CpdR and ClpX that impact CpdR-ClpX binding. The putative CpdR mutants K101A and S12A did not seem to be important for ClpX binding, and mutating the H104 residue to another residue capable of coordinating zinc did not recover the H104A phenotype. The inability to recover the H104A phenotype seems to indicate that the H104 residue is not in fact important in coordinating zinc at the NTD of ClpX, and may bind ClpX in another way. While the CpdR mutants did not show an effect on ClpX binding, the ClpX mutants identified by CollabFold seem to show a reduction in binding as shown by a reduction in both the number of blue colonies and the overall saturation of

blue coloration upon resuspending the whole population of cells. Moving forward, purifying these two ClpX mutants in vitro and validating a reduction in CpdR-mediated delivery would help to validate the observed reduction in binding by BACTH.

In terms of the ClpX mutants generated from the previously identified SspB mutants, while the NMR data indicated an importance of the A29 residue in E. coli ClpX, based on degradation reactions there was not a difference in terms of fold activation of SspB mediated delivery between wild-type and A29N ClpX. When reconstituted with CpdR, a similar effect was observed. Interestingly, while the A29N mutant was purified the same method as wild-type, the overall yield was much higher. Normally for WT ClpX the yield ranges from 4-10 uM as a hexamer, this mutant was purified at 24.4 uM as a hexamer, which is roughly 4 times the concentration as normal for wild-type ClpX. Moving forward, given that this mutant does not seem to be impacted by CpdR-mediated delivery, it may be a useful tool for performing other types of biophysical assays such as HDX-MS to identify specific binding residues between ClpX and CpdR. In the past, inability to purify WT ClpX to high concentrations has been a limiting factor when attempting to identify binding interfaces between CpdR and ClpX using methods such as HDX-MS or NMR. This mutant version may be a useful tool to be able to overcome previous concentration limitations in experimental design.

CHAPTER 3

MAGNESIUM-DEPENDENCE OF CLPX SUBSTRATE DEGRADATION

3.1. Introduction – The importance of Magnesium Coordination In Response Regulators

It is understood that response regulators undergo conformational changes upon phosphorylation. The phosphorylation at the conserved aspartic acid residue interacts with conserved portions of the receiver domain active site, and helps to coordinate a metal ion, specifically magnesium, at the conserved cluster of aspartic acid residues. When phosphorylated, the α4β5α5 face of the receiver domain undergoes the largest conformational change, such that phosphorylation results in a change in signaling output function (Bourret, 2010). In CpdR, phosphorylation at the D51 residue results in a conformational change that renders the response regulator inactive, while for CheY, phosphorylation is activating in terms of function (Figure 3-1). Phosphorylation for both proteins requires a divalent cation in order to add or remove the phosphoryl group, and it is thought that the binding affinity for the divalent cation increases upon phosphorylation, and vice-versa. Due to the importance of magnesium in regulating CpdR phosphorylation, and thus activity, we wanted to directly test the role in which magnesium regulates CpdR function *in vitro*. We assessed the impact of magnesium using fluorescent degradation assays and thermal shift assays.

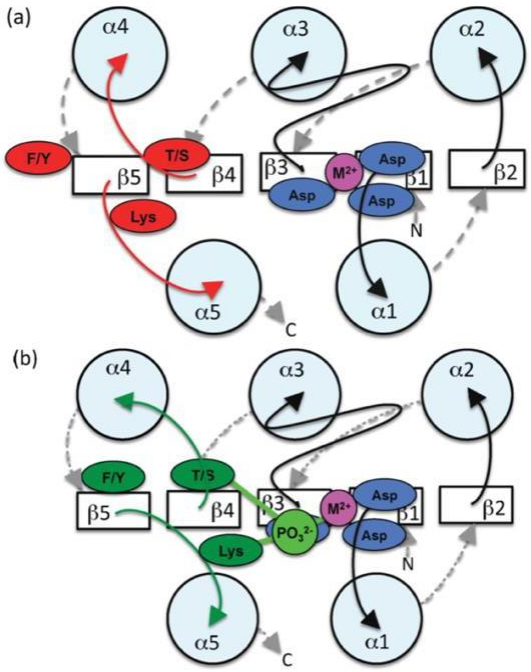

Figure 3-1. Phosphorylation-mediated conformational changes regulates response regulator function Bourret , 2010)

3.2. Magnesium Regulates ClpX Substrate Degradation *in vitro*.

To begin assessing the role that magnesium may play in regulating CpdR binding to ClpX, we first performed titrations of Magnesium at increasing concentrations with substrates that required CpdR and substrates that were natively degraded by ClpX alone. To start, we monitored substrate degradation of GFP-SsrA which is degraded by ClpX alone, and GFP-PdeA which requires CpdR for degradation to occur (Figure 3-2A). Interestingly, we observed that at increasing concentrations of magnesium, the degradation rate of GFP-SsrA increased at increasing concentrations of Mg^{2+} (Figure 3-2B). On the other hand, for CpdR-mediated delivery, GFP-PdeA degradation rate increased up to 10 mM Magnesium, however, upon addition of higher levels of Magnesium, the degradation rate decreased (3-2B). To ensure that the differences in regulation of CpdR-mediated delivery and ClpX-mediate delivery were due to magnesium concentration alone, we also performed the same titration with a substrate that is capable of being degraded by ClpX alone, but

whose degradation is amplified when CpdR is present. We utilized GFP-PAS-SsrA (Figure 3-3A), which contains the PAS domain of CpdR such that adding CpdR

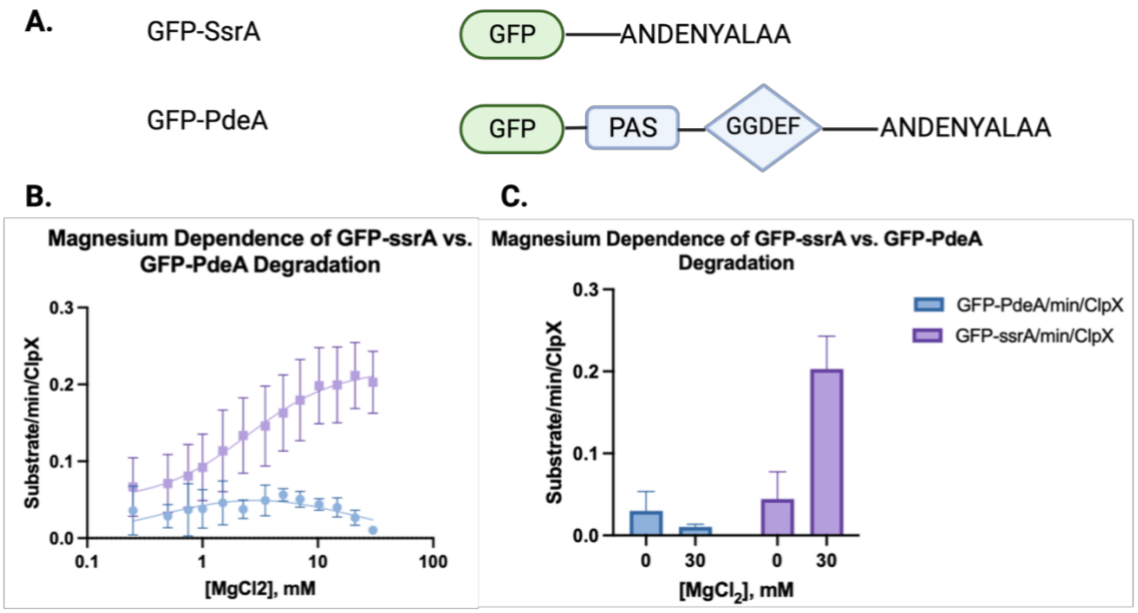

Figure 3-2. Magnesium Regulates ClpX Substrate Degradation *in vitro*. A. Two substrates were utilized for observation of the role of magnesium in substrate degradation. GFP-SsrA was purified for the observation of CpdR-independent degradation, while GFP-PdeA was purified for the observation of CpdR dependent degradation. B. Magnesium chloride was titrated at increasing concentrations from 0 $MgCl_2$ added to 30 mM $MgCl_2$ added. Reactions were performed at 0.4 uM ClpX (Hexamer), 0.8 uM $ClpP_{14}$ (tetradecamer), 2 uM substrate, with ATP regeneration mix. When present, 2 uM adaptor and 1 mM GTP were added. Degradation reactions were observed over the course of 30 minutes on a Spectramax M5 (Molecular Devices) microplate reader with excitation wavelength 460nm, emission wavelength at 540nm, and a cutoff of 515 nm

increases substrate degradation rate. When we titrated magnesium in the presence and absence of CpdR with this substrate, we observed a similar affect as GFP-PdeA. In the absence of CpdR, GFP-PAS-SsrA degradation was activated at increasing concentrations, with activation showing a plateau at the highest concentrations of magnesium (Figure 3-3B), while in the presence of CpdR increasing concentrations of magnesium resulted in an overall inhibition at increasing concentrations of magnesium (Figure 3-3C). Once we validated that the difference in magnesium regulation of CpdR-delivery was not due to differences in the substrate being used, we wanted to

compare the effect of magnesium between WT CpdR and CpdR (D9G). In theory, D9G is thought to be a magnesium blind mutant of CpdR, such that CpdR (D9G) would be expected to show differences in magnesium inhibition as compared to WT CpdR. Using a GFP-tagged

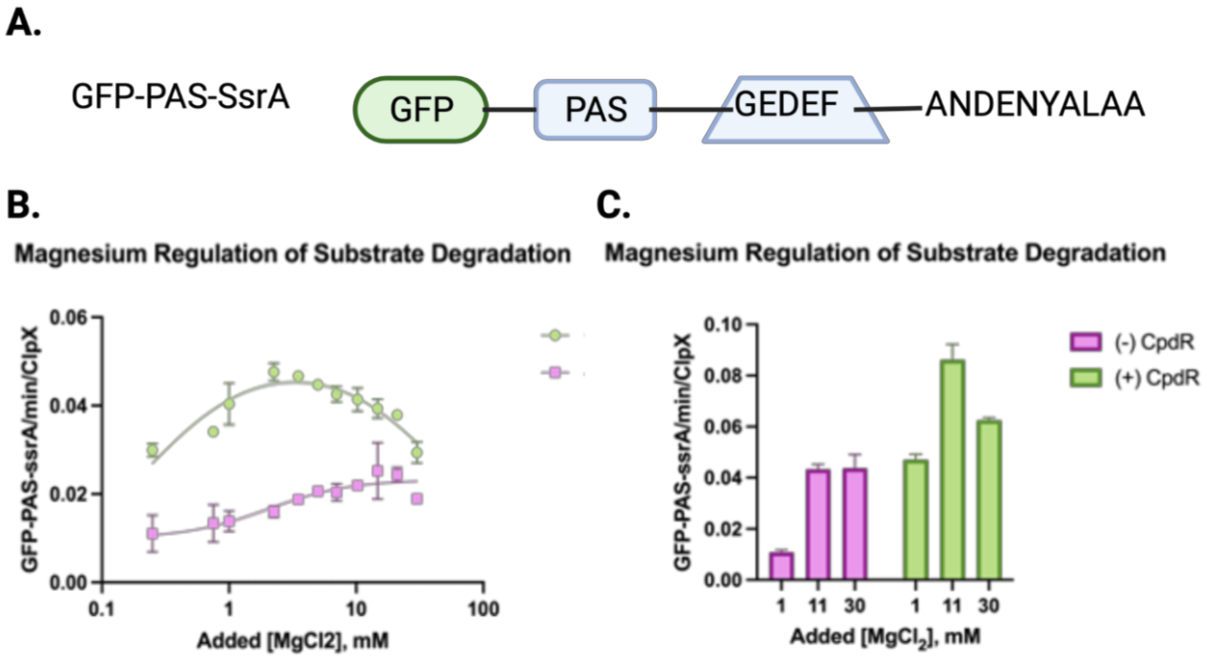

Figure 3-3. Magnesium Regulation is not substrate dependent. A. GFP-PAS-SsrA was utilized to compare the effect of magnesium on CpdR-Dependent degradation. B. Magnesium chloride was titrated at increasing concentrations from 0 $MgCl_2$ added to 30 mM $MgCl_2$ added. Reactions were performed at 0.4 uM ClpX (Hexamer), 0.8 uM $ClpP_{14}$ (tetradecamer), 2 uM substrate, with ATP regeneration mix. When present, 2 uM adaptor and 1 mM GTP were added. Degradation reactions were observed over the course of 30 minutes on a Spectramax M5 (Molecular Devices) microplate reader with excitation wavelength 460nm, emission wavelength at 540nm, and a cutoff of 515 nm

truncation of PdeA including only the first 265 amino acids attached to a degron tag (Figure 3-4A), we characterized the inhibition profiles of both wild-type CpdR and CpdR (D9G). Upon titration of magnesium, both CpdR and CpdR (D9G) were observed to show very similar inhibition profiles (Figure 3-4B). While CpdR (D9G) showed overall more activity as compared to WT CpdR which is consistent with previous findings, the overall inhibition of CpdR (D9G) by magnesium was very similar to that of WT CpdR.

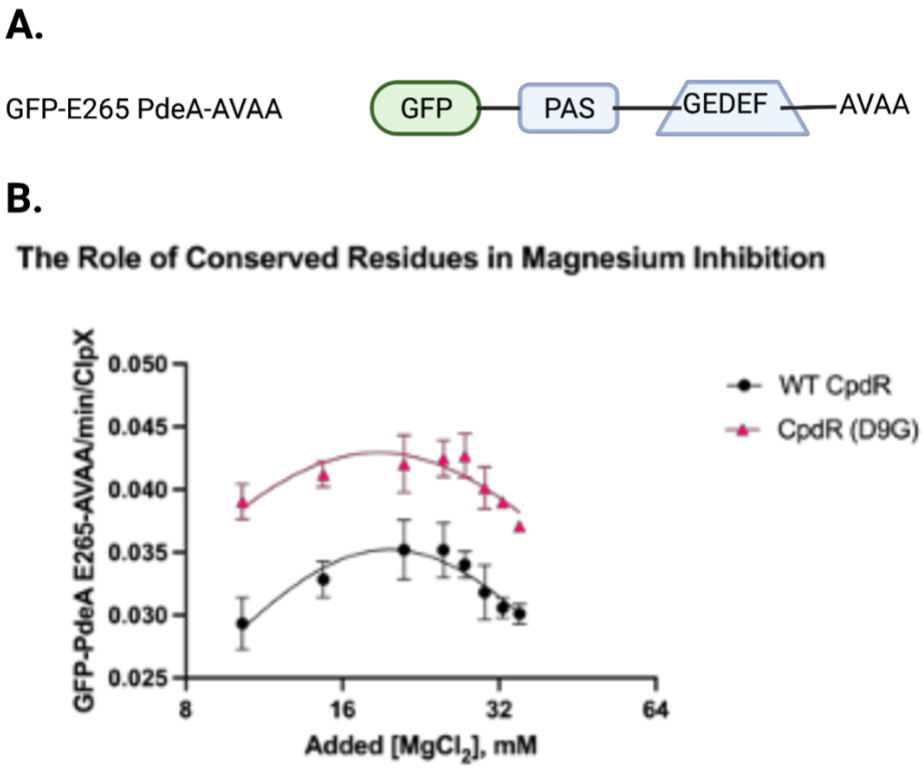

Figure 3-4. Magnesium Inhibition Profiles of CpdR vs. CpdR (D9G). A. GFP-E265-PdeA-AVAA was utilized to compare the effect of magnesium on WT CpdR and CpdR (D9G). This construct contains a GFP-tagged truncation of PdeA with an AVAA degron at the C-terminus. B. Magnesium chloride was titrated at increasing concentrations from 0 $MgCl_2$ added to 30 mM $MgCl_2$ added. Reactions were performed at 0.4 uM ClpX (Hexamer), 0.8 uM $ClpP_{14}$ (tetradecamer), 2 uM substrate, with ATP regeneration mix. When present, 2 uM adaptor and 1 mM GTP were added. Degradation reactions were observed over the course of 30 minutes on a Spectramax M5 (Molecular Devices) microplate reader with excitation wavelength 460nm, emission wavelength at 540nm, and a cutoff of 515 nm

3.3. Conclusions and Future Directions

Based on our fluorescent degradation assays, magnesium seems to play a role in regulating substrate degradation. While magnesium plays an activating role in degrading substrates that do not require an adaptor in order to be degraded, there is an apparent inhibition of substrate degradation for substrates that require CpdR to be present. Based on our CollabFold model, the D9 residue on CpdR that coordinates magnesium seemed to be oriented toward the K53 residue on ClpX, and based on our BACTH data mutating K53 to a negatively charged residue seemed to

reduce binding to CpdR. Thus, magnesium binding at this site may not only play a regulatory role in phosphorylation, but additionally may directly block binding to ClpX. Since our purifications of CpdR lack the canonical phosphorylation system required for CpdR phosphorylation, it is likely that magnesium is directly blocking binding rather than strengthening the phosphorylated state (Figure 3-5). However, when comparing CpdR (D9G) to WT CpdR, there was no significant difference in terms of the magnesium inhibition profiles, which could be a result of a number of factors. First, it could be that mutating one aspartic acid residue is not sufficient to prevent magnesium coordination at this cluster of aspartic acid residues, such that magnesium can still directly inhibit binding. On the other hand, magnesium could be playing a regulatory role that is unrelated to the coordination of magnesium at the conserved cluster of aspartic acid residues, and functions to alter CpdR binding in another way. To solidify that magnesium plays a direct role in binding, biophysical assays will be required to determine how CpdR affects direct binding rather than using degradation as a proxy for binding strength.

CHAPTER 4

BIOPHYSICAL METHODS OF UNDERSTANDING CPDR BINDING OF NTD CLPX

4.1. Introduction – The Limitations of Studying ClpX in a Biophysical Context

ClpX historically is a protein that is extremely difficult to purify. Previous students who have worked on the adaptor hierarchy system face the same issue: ClpX is limited by its instability at high concentrations and at a sufficient purify, such that biophysical methods of understanding CpdR-ClpX binding have remained elusive. In my project, I aimed to attempt to understand CpdR-ClpX binding at a biophysical level using a plethora of methods, including Isothermal Calorimetry (ITC), Differential Scanning Fluorimetry (DSF), and HDX-MS to try to understand both the kinetic parameters of binding as well as the specific residues involved in binding. Due to concentration and purity limitations with full-length ClpX, I attempted these methods using a truncation of the NTD of ClpX, the minimal region required for CpdR binding.

4.2. Using Isothermal Calorimetry to Identify Direct Binding with CpdR and NTD ClpX

In an effort to understand the kinetic binding parameters between ClpX and CpdR, I preformed Isothermal Calorimetry (ITC) to try to characterize the binding interaction between ClpX and CpdR. I titrated NTD ClpX or buffer into CpdR, and observed the change in heat over time between titrations. The change in heat over time of buffer injections remained constant and resulted in. very little heat change (Figure 4-1). While the change in heat per second did decrease over time as more and more NTD was added, the binding reaction never reached saturation, such that I was unable to calculate the binding parameters of binding (Figure 4-1). I attempted to purify the NTD again in the millimolar concentration range, however, due to instability at high concentrations I was unable to do so.

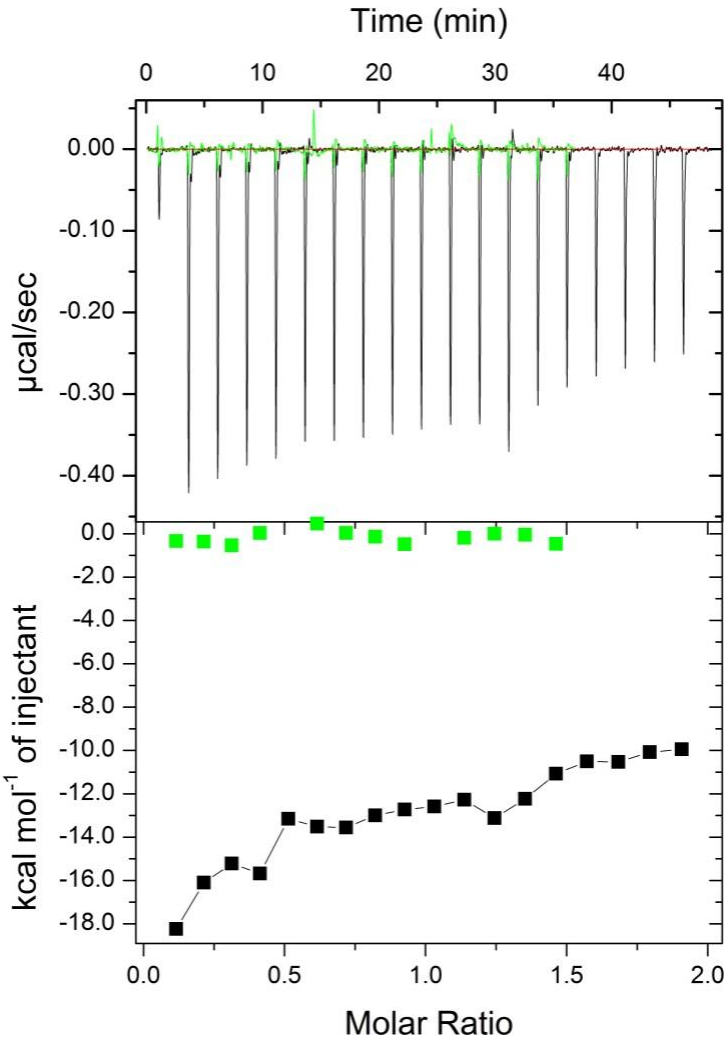

Figure 4-1. Isothermal Calorimetry of CpdR and NTD ClpX. 100 uM NTD ClpX was titrated into 10 uM CpdR both stored in H-buffer (20 mM HEPES, pH 7.5, 100 mM KCl, 10 mM $MgCl_2$, 10% Glycerol). Injections were performed at volumes of 2 uL over the course of 19 injections. Injections using H-buffer were performed as a negative control.

4.3. Using Differential Scanning Fluorimetry to understand How CpdR Impacts ClpX Upon Binding

To understand how CpdR binding impacts ClpX function as a protease, I performed Differential Scanning Fluorimetry. I mixed Sypro orange hydrophobic dye with both CpdR alone, NTD alone, and both CpdR and NTD mixed in solution. I then observed the thermal unfolding of each sample

at increasing temperature over time. If CpdR stabilizes NTD ClpX in some conformational way, we may expect the melting temperature of NTD to be stabilized in the presence of CpdR. Interestingly, when exposed to CpdR, the N-terminal domain of ClpX exhibits a higher melting temperature as compared to NTD alone (Figure 4-2). While NTD alone observed a melting temperature of approximately 51^{o}C, the thermal unfolding curve of both CpdR and NTD alone exhibited a much higher melting temperature, at about 70^{o}C. This indicates that CpdR binding is stabilizing ClpX as a protease in some conformational way.

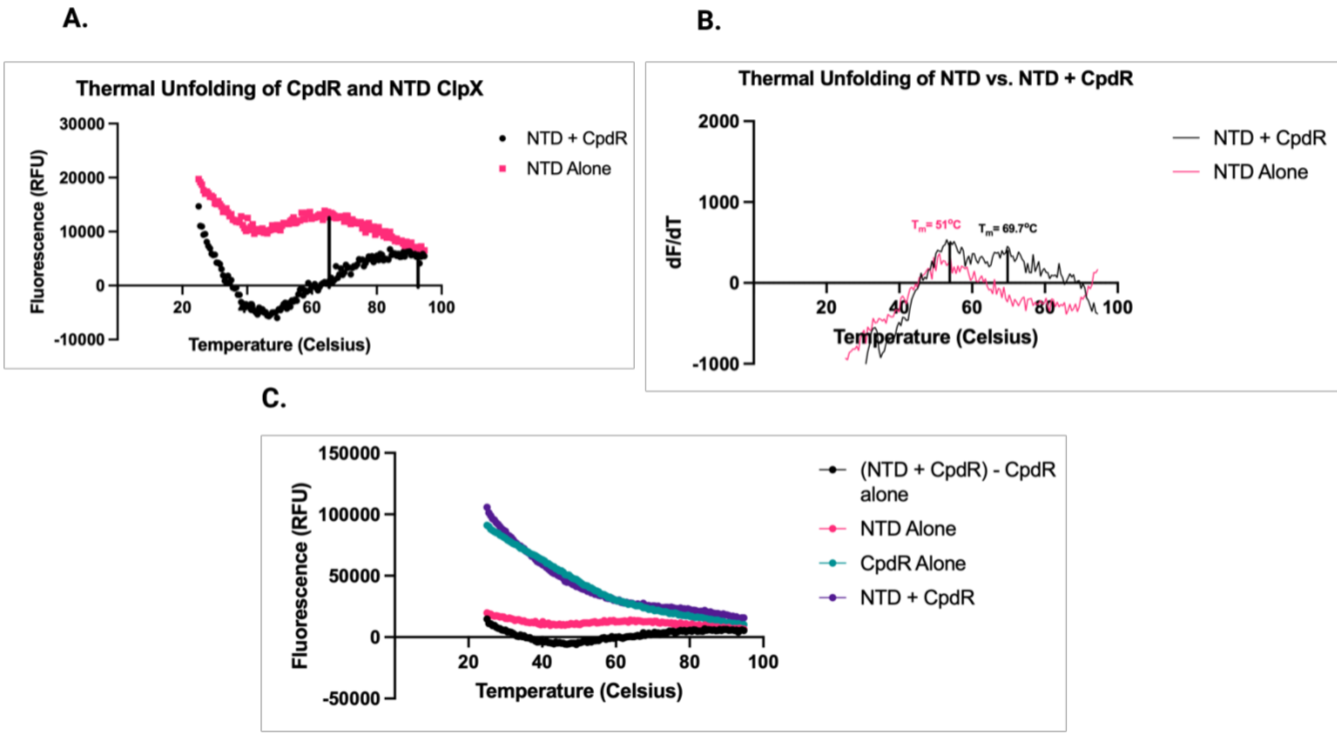

Figure 4-2. CpdR Stabilizes NTD ClpX Upon Binding. Thermal unfolding of CpdR alone, NTD ClpX alone, or CpdR and NTD in solution was observed over a temperature gradient from 25°C to 95°C. Adaptor and protease at concentrations of 4 uM and 50 uM, respectively, were exposed to 4X Sypro orange at room temperature over the course of 30 minutes prior to temperature gradient. After 30 minutes of incubation, temperature was ramped using a QuantStudio 7 Real-Time PCR system (Thermo Fisher Scientific) at increments of 0.16°C/min, with a final hold at 95°C. A. Normalized melt curves of NTD + CpdR and NTD Alone were generated by subtracting the background fluorescence of CpdR alone from NTD + CpdR. B. The first derivative of the normalized melt curve of NTD alone and CpdR + NTD was taken and plotted against the temperature gradient. The melting temperatures were calculated as the temperature at which we

observed the highest peaks of dF/dT. C. Raw Fluorescence data of each sample was plotted against the temperature gradient.

4.4. Hydrogen Deuterium Mass Spectrometry (HDX-MS) of CpdR and NTD ClpX

To understand the specific residues and regions that are involved in CpdR:ClpX binding, I performed HDX-MS. When designing the experiment, while we were initially interested in understanding the residues on ClpX that were important for CpdR binding, due to concentration limitations of CpdR, we decided to use NTD ClpX at the highest concentration of 30 uM post-quenching, and have CpdR at a final concentration of 1 uM post-quenching. Because of the way we set up the experiment, we would expect to see the protection on the CpdR peptides more than we would see on the NTD peptides, as CpdR would be predicted to be saturated with NTD, while NTD would not be expected to be saturated by CpdR at limiting CpdR concentrations. Because previous work has shown that it seems like the CpdR-NTD interaction is weak and thus possibly very dynamic, we decided to perform short labeling times, as we would predict to see any changes within the first few minutes of labeling. To this end, we chose labeling times of 0, 10, and 120 seconds in triplicate for each condition. After pruning the mass spec data and manually selecting peaks for each charge state for each peptide, we analyzed the uptake by heatmap. Interestingly, when the NTD ClpX was exposed to CpdR, it appeared as though there was an overall protection in the region at amino acids residues 19 – 35 on the N-terminal domain of ClpX. Conversely, there seemed to be an overall exposure within the region of amino acids 49 – 55 (Figure 4-3A). We found this interesting as based on our BACTH data, mutating the residue E24K seemed to result in a consistent deficiency of binding based on the beta-galactosidase activity when plated on X-gal (Figure 2-3). Conversely, the K53E mutant was less consistent, and when repeated appeared to look like wild-type ClpX (Figure 2-4). Both of these observation in a bacterial-two hybrid system are consistent with the observed protection and exposure at

these sites on ClpX. When mapping the regions of protection onto the AlphaFold2 predictions, these regions appear to be consistent with both regions of exposure and protect (Figure 4-4).

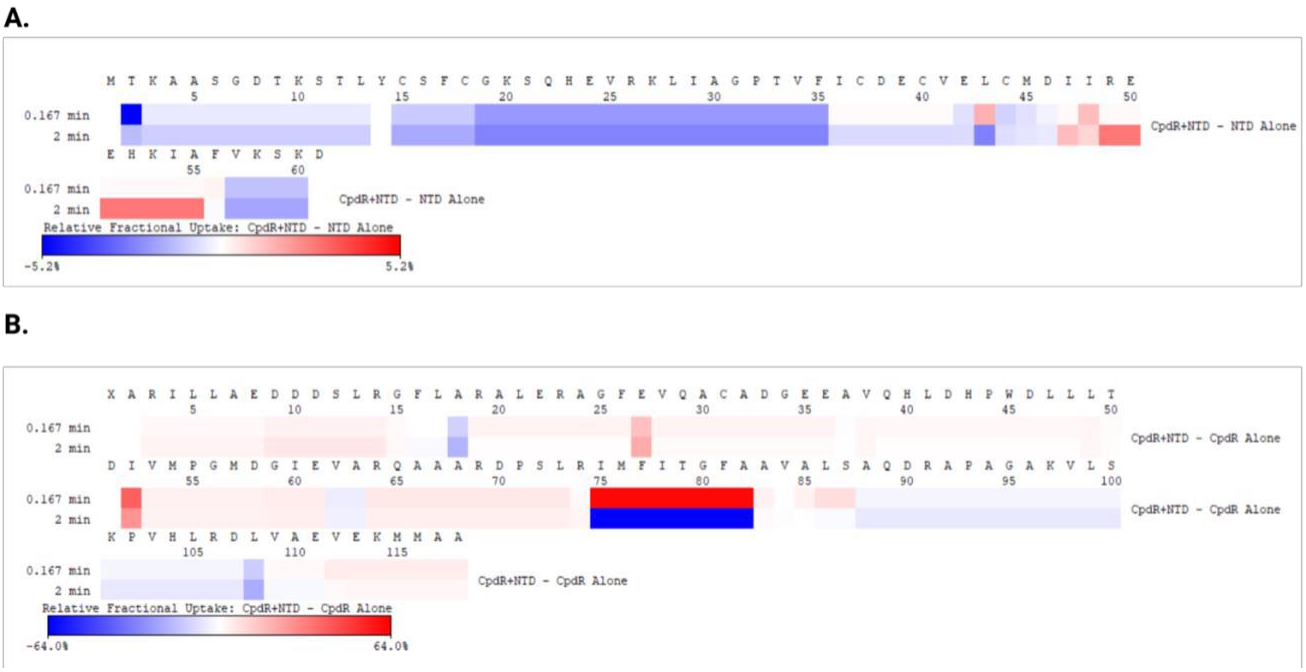

Figure 4-3. Heat Map of Relative Fractional Uptake on NTD ClpX. A. Stacked spectral uptake plots were mapped onto NTD sequence such that regions of uptake across the sequence were observable. Relative fractional uptake ranged from -5.26 to 5.26, with dark blue indicating protection and dark red indicating over exposure. B. Stacked spectral uptake plots were mapped onto CpdR sequence such that regions of uptake across the sequence were observable. Relative fractional uptake ranged from -64.04 to 64.04 with dark blue indicating protection and dark red indicating over exposure.

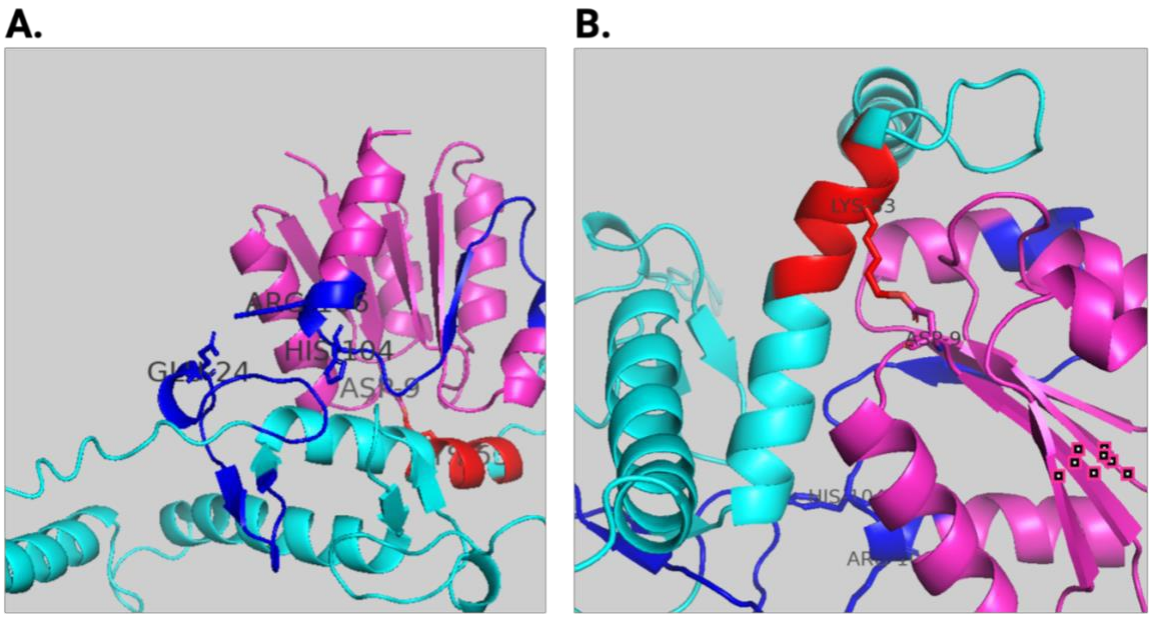

Figure 4-4. Plotting Relative Fractional Uptake of NTD onto AlphaFold2 Model. A and B. Regions of protection and high uptake were plotted onto the AlphaFold2 predictive model. CpdR is shown in pink, while NTD ClpX dimer is shown in light blue and light green. Regions that are highlighted in red are indicative of regions of high uptake, while regions highlighted in dark blue are indicative of protected regions.

When looking at the spectral uptake on the CpdR peptides in the presence of NTD ClpX, there was one region that seemed to show high variability between 10 seconds and 2 minutes of exposure, that had a very high relative fractional uptake in both directions (Figure 4-3B). However, upon investigation of the individual spectral uptake plots, it was clear that one plot clearly was skewing the data. Specifically, a single peptide ranging from amino acids 65-94 showed high relative uptake of approximately 30 Da at 10 seconds of exposure, but showed a severe reduction at 2 minutes of exposure (Figure 4-5A). This contrasted with other data surrounding that peptide, which all typically showed lower uptake ranging from 5-10 Daltons. Because of this, we think that this peptide is not representative of the true uptake at this location, and is likely contributing noise to our data. However, due to the consistency in the other peptides in the sequence, it is more likely that the other regions on the CpdR sequence are more accurate.

For example, from amino acids 88 – 108, there seemed to be an overall protection at this region (Figure 4-3B) This uptake data would be consistent with previous work showing that residues H104 and R106 are important for CpdR-mediated degradation of substrates, and thus binding to ClpX. When plotting this region onto CpdR, the region of protection in the amino acid region of 88 – 108 seems to align with the protection on NTD ClpX at about 19-35 (Figure 4-5B). The regions of exposure and protection for both CpdR and NTD ClpX seem to align well with our predictive model.

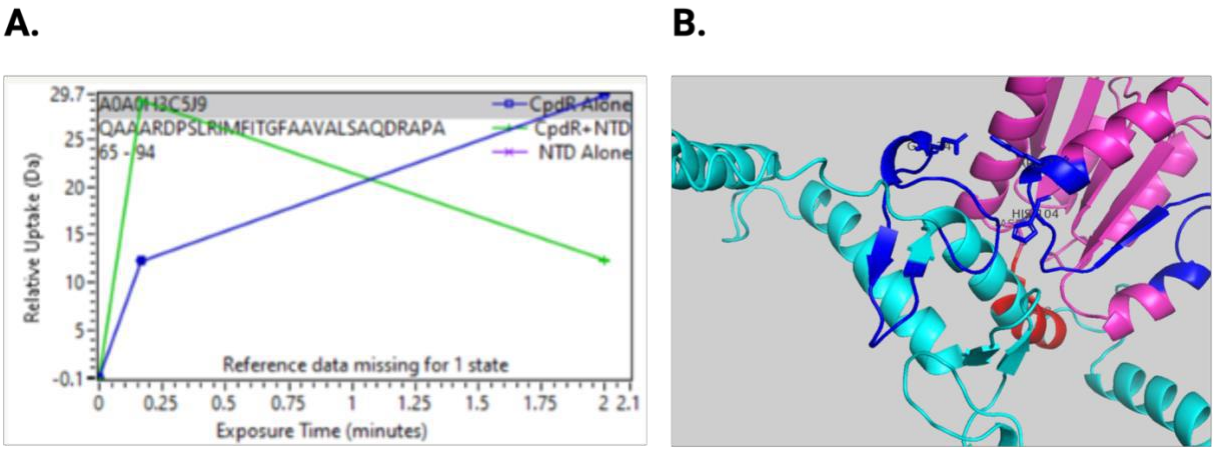

Figure 4-5. Plotting Fractional Uptake of CpdR onto AlphaFold2. A. Relative Uptake Plot of one CpdR peptide skews the uptake at one region. While the other uptake plots around this region showed very little change (see Appendix 2), one peptide appeared to show high variability and high uptake. B. Regions of protection and exposure were plotted onto the CpdR structure in the AlphaFold2 prediction model. CpdR is shown in pink, while NTD dimer is shown in light blue and green. Regions of protection are shown in dark blue, while regions of exposure are shown in dark red.

4.5. Conclusions and Future Directions

Given the limitations of purifying ClpX to high concentration, further work will be required to fully understand the biophysical parameters of CpdR binding to ClpX. While the ITC titration was not able to produce interpretable binding kinetic information, it does provide a basis to understand that CpdR is in fact binding to the N-terminal domain of ClpX. The observed

increase in melting temperature of NTD in complex with CpdR tells us that CpdR is in fact stabilizing ClpX in some conformational way that stabilizes the protease. Possibly increasing the amount of magnesium in the purification process for the NTD may stabilize the protein such that it can be purified to millimolar levels for more conclusive kinetic studies.

CHAPTER 5

PROJECT CONCLUSIONS AND FUTURE DIRECTIONS

5.1. A Model of CpdR binding to ClpX

Several observations from this work seem to indicate that magnesium plays a role in regulating CpdR binding to ClpX. First, when titrating magnesium at increasing concentrations, CpdR-mediate degradation seems to be inhibited, while ClpX mediated degradation is conversely activated. We know that mutation CpdR (D9G) shows higher activity *in vitro*, and seems to be resistant to phosphorylation. It could be that magnesium binding at this site plates a direct role in inhibiting CpdR binding to ClpX. Conversely, magnesium could be regulating CpdR at a level that is not understood currently, and would require further investigation. Through our bacterial-two hybrid screening in complementation with our HDX-MS data, it seems clear that E24 and the region surrounding it on ClpX seems to be important in binding CpdR, as shown by the overall protection at this region in our HDX data as well as the deficiency in beta galactosidase activity of this mutant by BACTH. These observations together provide a region of ClpX which we can focus on further to identify the interactions on ClpX that are important for CpdR binding. Characterizing E24K *in vitro* will be necessary to see if this region directly impacts substrate delivery.

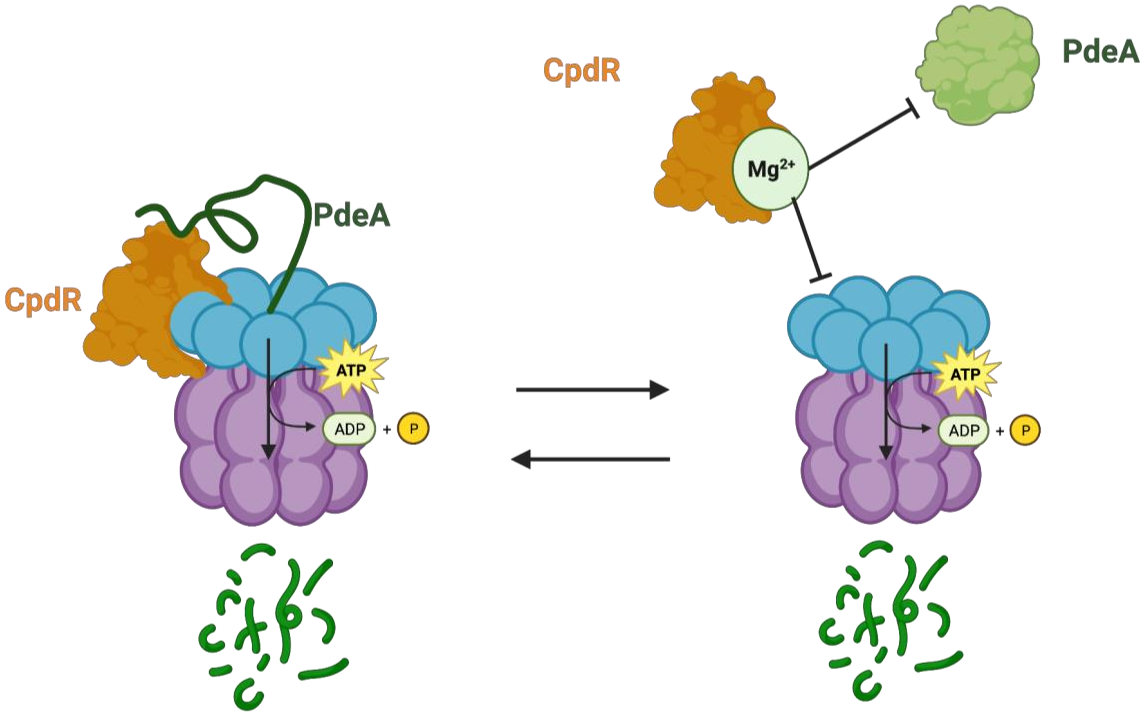

Figure 5-1. A Working Model of Magnesium Regulation of CpdR-Mediated Substrate Delivery in *Caulobacter Crescentus*. Magnesium coordination in response regulators is required for phosphorylation to occur, and phosphorylation strengthens Magnesium binding, and vice-versa. When CpdR is bound to magnesium, there is a physical block in binding to ClpX. When magnesium is released from the cluster of aspartic acid residues, CpdR is able bind the N-terminal domain of ClpX and prime the protease for substrate delivery.

5.2. Future Directions to understand Magnesium Regulation of CpdR and Mechanism of CpdR priming of ClpX

Given that we explored magnesium regulation of CpdR-ClpX binding *in vitro*, successfully executing biophysical binding experiments at increasing concentrations of magnesium is necessary to fully understand how magnesium impacts binding. One method that would be useful and would require very little sample is Microscale Thermophoresis (MST). Using a fluorescently tagged CpdR construct, we could monitor how magnesium impacts CpdR binding to either NTD ClpX or full-length ClpX. Another option would be to optimize the purification of the NTD ClpX using increased salt concentrations in an effort to stabilize and purify the protein into the millimolar range for ITC. Lastly, due to our success with identifying regions using HDX-

MS, varying the concentrations of magnesium and analyzing binding by HDX-MS in varying concentrations of magnesium could help us to understand exactly how magnesium regulates CpdR:ClpX binding.

APPENDIX A

MATERIALS AND METHODS

Bacterial strains

E. coli Top10 cells were used for cloning and stable storage of vectors. BL21 (DE3) cells were used to express recombinant proteins under control of a T7- isopropyl-beta-D-thiogalactopyranoside (IPTG) inducible promoter. BACTH *E. coli cya clpX* strain (EPC452, F- , *cya-99, araD139, galE15, galK16, rpsL1 (Str^r), hsdR2, mcrA1, mcrB1, ΔclpX*) was generated in previous work (Lau et al., 2016) and utilized in BACTH interaction studies.

Plasmid Constructions

Point mutants generated in both BACTH plasmids and expression vectors (pET23) were generated using around-the-horn cloning. Primers were designed in opposite directions from the site of mutation and contained 5'-phosphorylated ends. PCR amplification was executed in 50 uL reactions containing 0.5 uM of both forward and reverse primers, 10 mM dNTPs, 1X GC Buffer, 3% DMSO, 50 mM betaine, 1 units Phusion/50 uL PCR, and 2-10 ng template DNA.

In vitro degradation assay and ATPase reaction

Degradation assays using recombinant protein components were performed in H- Buffer (20mM HEPES, pH 7.5, 100mM KCl, 10mM $MgCl_2$, 10% glycerol, 5mM β-mercaptoethanol) at 30°C. In general, concentrations were 0.4μM ClpX (hexamer concentration), 0.8μM $ClpP_{14}$, in the presence of 4mM ATP (+ regeneration system), 2μM adaptors, 2μM substrates. For CpdR-mediated degradation reactions, 1 uM GTP was added. GFP-tagged substrate degradation was monitored in a 384-well black plate using a Spectramax M5 (Molecular Devices) microplate reader with excitation wavelength 460nm, emission wavelength at 540nm, and a cutoff of 515 nm. ATPase reactions of WT ClpX and A29N mutant were performed using increasing concentrations of ATP (0-1mM) with 0.16 uM ClpX (hexamer), 0.1 uM ClpX (tetradecamer), and 1 uM substrate.

Bacterial Adenylyl Cyclase Two-Hybrid (BACTH) assay

CpdR-ClpX interactions were surveyed using BACTH (Karimova et al., 1998). CpdR mutants were generated from a wild-type T25-CpdR vector using around- the-horn cloning. ClpX mutants were generated from T18C-WT ClpX using around-the-horn cloning. Mutants were validated by nanopore sequencing (Plasmidsaurus). Various combinations of WT and Mutant T25-CpdR and T18C- ClpX were transformed into chemically competent BTH101 ΔClpX cells. BACTH

transformants were analyzed by plating cells on media containing 0.2 mg/mL X- gal and 0.2mg/mL IPTG with 100 ug/mL Amp and 50 ug/mL Kan.

Protein purification by affinity chromatography

Proteins for purification were overexpressed from IPTG-inducible pET23 vectors and purified as previously reported (Rood et al., 2012; Bhat et al., 2013; Lau et. al, 2016). CpdR, CpdR (D9G), NTD ClpX, SspB, and substates were purified as C- terminal His-SUMO fusions expressed in BL21 (DE3) cells. His_6SUMO tag fusion was cleaved by Ulp1 digestion overnight at 4^oC during dialysis. Proteins were

separated by subtractive nickel, and NTD and CpdR were further purified using a Superdex 75 10/300 Size-Exclusion Chromatography column (GE Healthcare).

Differential Scanning Fluorimetry (DSF)

Thermal unfolding experiments were performed in a QuantStudio 7 Pro real-time PCR system (ThermoFisher Scientific) in clear 384-well plates (corning).

Reactions were performed at 20 uL volumes, with adaptor and protease at

concentrations of 4 uM and 50 uM, respectively. Samples were exposed to 4X Sypro Orange (Invitrogen) for 30 minutes in a dark space at room temperature to allow for pre-incubation, prior to a temperature gradient from 25°C to 95°C, with

ramping increments of 0.16°C/min. Samples were kept at a final hold of 95°C for 2:00 min.

Isothermal Calorimetry (ITC)

Isothermal Calorimetry experiments were performed using a MicroCal Auto iTC_{200} (Malvern Instruments). CpdR was loaded into the sample cell at a starting concentration of 10 um, and NTD ClpX was loaded into the syringe at a starting concentration of 100 uM. Injections were performed at volumes of 2 uL over the course of 19 injections, with an initial priming injection of 0.4 uL. Injections using H-Buffer (20 mM HEPES, pH 7.5, 100 mM KCl, 10 mM $MgCl_2$, 10% Glycerol) were performed as a negative control.

CpdR CollabFold Modeling

CpdR and NTD predictive modeling was performed in CollabFold where the sequences of CpdR, RcdA, and NTD ClpX were entered as duplicates. The highest confidence model was selected to move forward with analysis.

Hydrogen Deuterium Mass Spectrometry (HDX-MS)

HDX-MS experiments were performed using a Synapt G2Si high-definition mass spectrophotometer (Waters) in triplicate for each CpdR alone, CpdR + NTD, and NTD Alone. Blank runs were performed in between samples to prevent peptide

carryover. Deuterium exchange and quenching steps were performed using an automated HDX liquid handler (Waters). Samples were diluted 1:16 in H-Buffer (20 mM HEPES, 100 mM KCl, 10 mM $MgCl_2$, 10% glycerol) containing 80% D_2O. Samples were allowed to exchange for 0, 10, and 120 seconds at 16^{O}C. At each timepoint, aliquots were diluted 1:2 in cold quench buffer at 4 ^{O}C (100 mM K_2HPO_4, pH 2.5) leaving CpdR and NTD ClpX at final concentrations of 1 uM and 30 uM, respectively. Post-quenching, samples were run over a Waters ENZYMATE immobilized pepsin column (inner diameter: 2.1 x 30 mm) at a flow rate of 0.15 mL/min at high pressure for peptide digestion. Identification of peptides and uptake analysis for each charge state and peptide were performed in Protein Lynx Global Server and DynamX (v. 3.0, Waters).

Plasmids used in this work

Plasmid Name	Description	Reference
pET23 His_6SUMO CpdR	For purification of full length CpdR (Amp^R)	(Abel et al., 2011)
pET23 His_6SUMO NTD ClpX	For purification of his-tagged NTD ClpX (1-61) (Kan^R)	(Lau et al. 2016)
pET23 *C. crescentus* ClpX	For purification of untagged *C. crescentus* ClpX (Amp^R)	(Bhat et al., 2013)
pET28bh6-delN9SspB	For purification of His_6-tagged SspB.	(Chien et al., 2007b)
pKT25 CpdR	*E. coli* plasmid for expressing T25-WT CpdR using P_{lac} (Kan^R)	(Lau et al., 2016)
pKT25 CpdR H104A	*E. coli* plasmid for expressing T25-CpdR H104A using P_{lac} (Kan^R)	(Lau et al., 2016)

pKT25 CpdR H104E	*E. coli* plasmid for expressing T25-CpdR H104E using P_{lac} (Kan^R)	This study
pKT25 CpdR H104C	*E. coli* plasmid for expressing T25-CpdR H104C using P_{lac} (Kan^R)	This study
pKT25 CpdR S12A	*E. coli* plasmid for expressing T25-CpdR S12A using P_{lac} (Kan^R)	This study
pKT25 CpdR K101A	*E. coli* plasmid for expressing T25-CpdR K101A using P_{lac} (Kan^R)	This study
pKT25 Empty Vector	*E. coli* plasmid for expressing T25-Empty using P_{lac} (Kan^R)	(Lau et al., 2016)
pUT18C – C. crescentus ClpX	*E. coli* plasmid for expressing T18C-ClpX using P_{lac} (Amp^R)	(Lau et al., 2016)
pUT18C-ClpX E24K	*E. coli* plasmid for expressing T18C-ClpX using P_{lac} (Amp^R)	This study
pUT18C-ClpX K53E	*E. coli* plasmid for expressing T18C-ClpX using P_{lac} (Amp^R)	This study
pUT18C-Empty	*E. coli* plasmid for expressing T18C-Empty using P_{lac} (Amp^R)	(Lau et al. 2016)
pET23-His_6SUMO CpdR D9G	For purification of CpdR D9G (Amp^R)	(Lau et al., 2016)
pET23-His_6SUMO E265	For purification of his-tagged truncation of PdeA (2-265) with AVAA degron attached	(Rood et al., 2012)
pET23 C. crescentus ClpX A29N	For purification of untagged *C. crescentus* Mutant ClpX (A29N) (Amp^R)	This study

375-His-eGFP-PdeA	For purification of his-tagged eGFP-PdeA (Amp^R)	(Rood et al., 2012)

Bacterial strains used in this work

Plasmid Name	Description	Reference
Top10	*E. coli* cloning strain	Invitrogen
BL21 (DE3) pLysS	*E. coli* strain for recombinant protein expression.	Invitrogen
BTH101 ΔClpX	*E. coli* BACTH reporter strain lacking functional cya (adenylate cyclase gene for expressing cAMP) and containing a markerless deletion of *clpX* using Flp-FRT recombination	(Lau et. al, 2016)

APPENDIX B

HYDROGEN DEUTERIUM MASS SPECTROMETRY SPECTRAL UPTAKE PLOTS

CpdR Spectral Uptake Plots

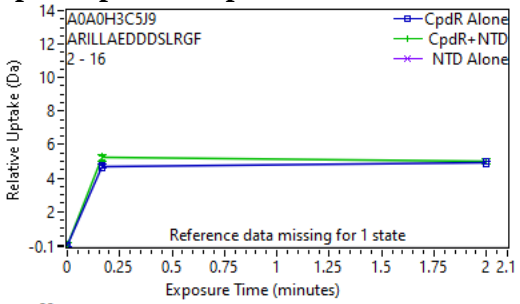

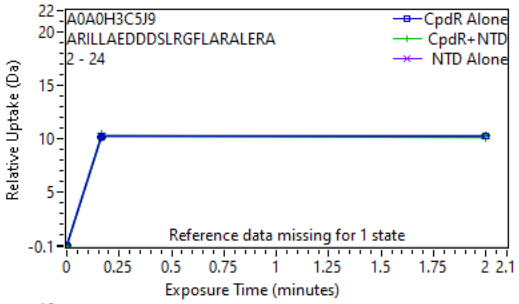

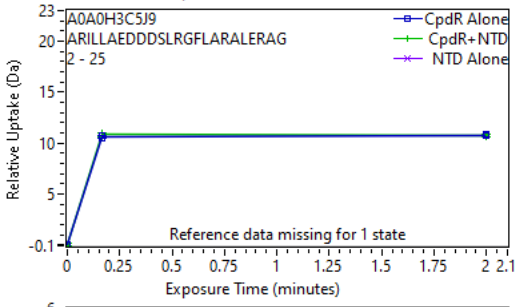

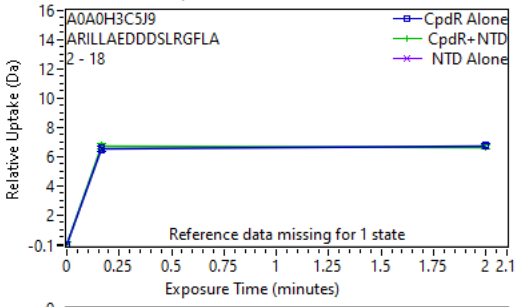

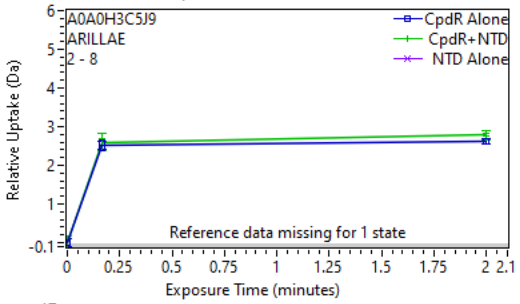

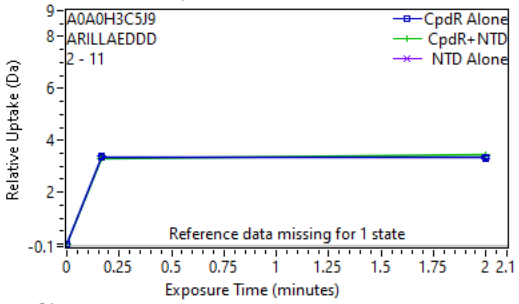

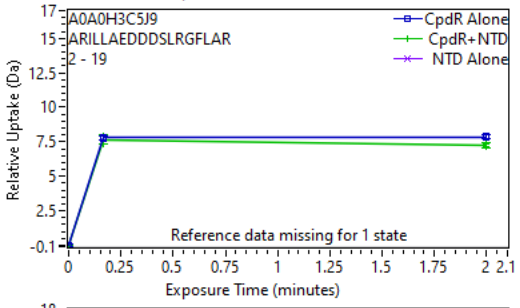

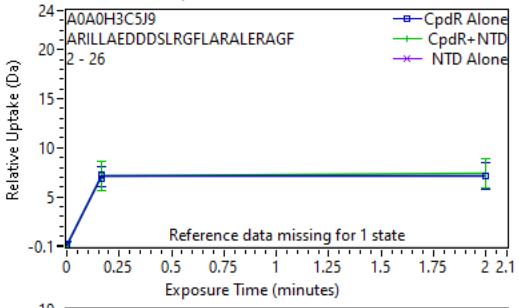

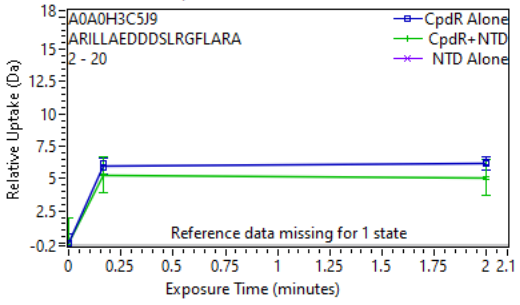

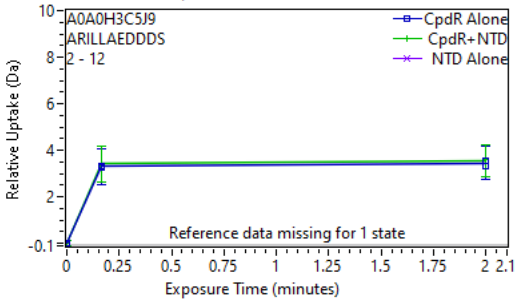

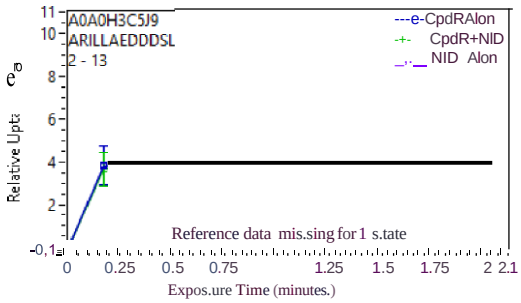
A0A0H3C5J9
ARILLAEDDDSL
2 - 13
---e-CpdRAlon
-+- CpdR+NID
_,-.__ NID Alon
Relative Uptx
Reference data mis.sing for 1 s.tate
Expos.ure Time (minutes.)

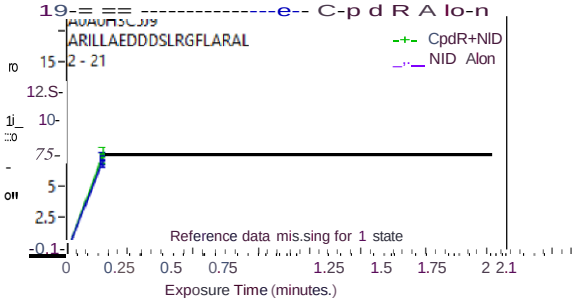
ARILLAEDDDSLRGFLARAL
2 - 21
-+- CpdR+NID
_,-.__ NID Alon
Reference data mis.sing for 1 state
Exposure Time (minutes.)

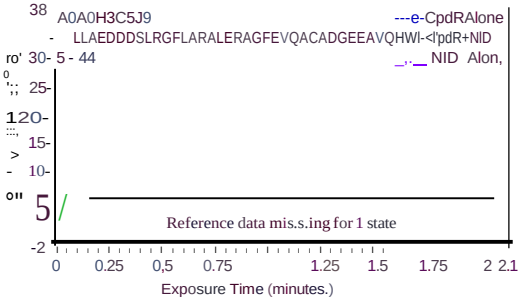
A0A0H3C5J9
LLAEDDDSLRGFLARALERAGFEVQACADGEEAVQHWI-<I'pdR+NID
30- 5 - 44
---e-CpdRAlone
_,-.__ NID Alon,
Reference data mis.s.ing for 1 state
Exposure Time (minutes.)

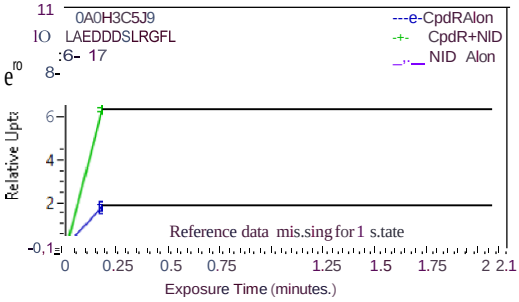
0A0H3C5J9
LAEDDDSLRGFL
:6- 17
---e-CpdRAlon
-+- CpdR+NID
_,-.__ NID Alon
Relative Uptx
Reference data mis.sing for 1 s.tate
Exposure Time (minutes.)

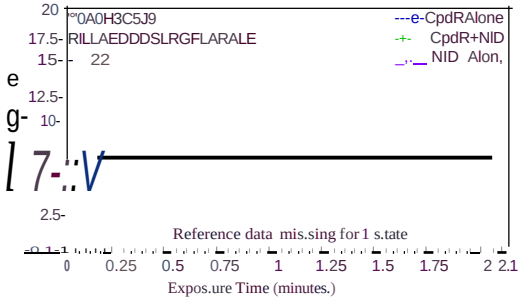
0A0H3C5J9
RILLAEDDDSLRGFLARALE
22
---e-CpdRAlone
-+- CpdR+NID
_,-.__ NID Alon,
Reference data mis.sing for 1 s.tate
Expos.ure Time (minutes.)

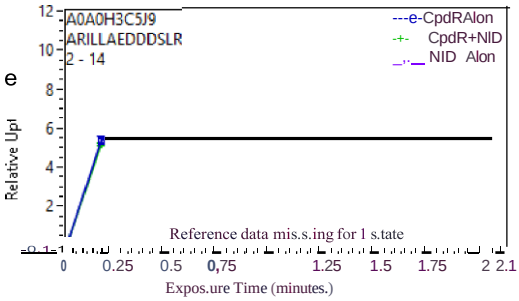
A0A0H3C5J9
ARILLAEDDDSLR
2 - 14
---e-CpdRAlon
-+- CpdR+NID
_,-.__ NID Alon
Relative Upt
Reference data mis.s.ing for 1 s.tate
Expos.ure Time (minutes.)

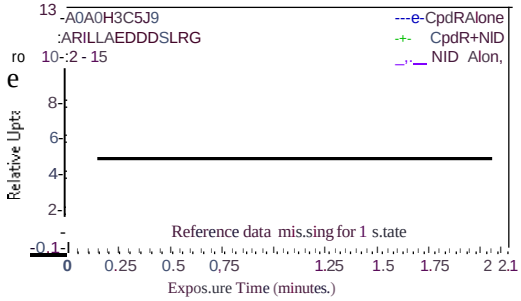
A0A0H3C5J9
:ARILLAEDDDSLRG
10-:2 - 15
---e-CpdRAlone
-+- CpdR+NID
_,-.__ NID Alon,
Relative Uptx
Reference data mis.sing for 1 s.tate
Expos.ure Time (minutes.)

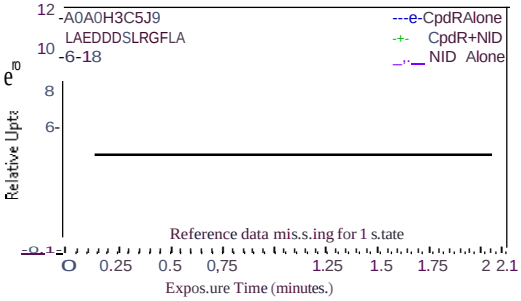
A0A0H3C5J9
LAEDDDSLRGFLA
-6-18
---e-CpdRAlone
-+- CpdR+NID
_,-.__ NID Alone
Relative Uptx
Reference data mis.s.ing for 1 s.tate
Expos.ure Time (minutes.)

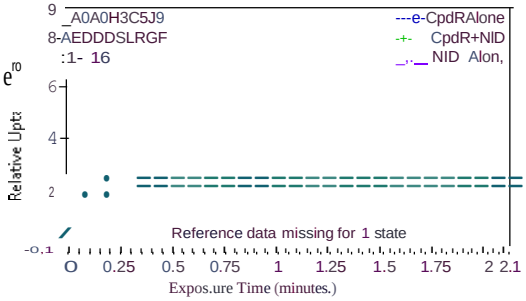
A0A0H3C5J9
8-AEDDDSLRGF
:1- 16
---e-CpdRAlone
-+- CpdR+NID
_,-.__ NID Alon,
Relative Uptx
Reference data missing for 1 state
Expos.ure Time (minutes.)

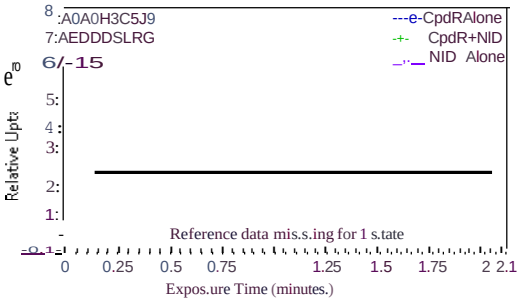
A0A0H3C5J9
7:AEDDDSLRG
6/-15
---e-CpdRAlone
-+- CpdR+NID
_,-.__ NID Alone
Relative Uptx
Reference data mis.s.ing for 1 s.tate
Expos.ure Time (minutes.)

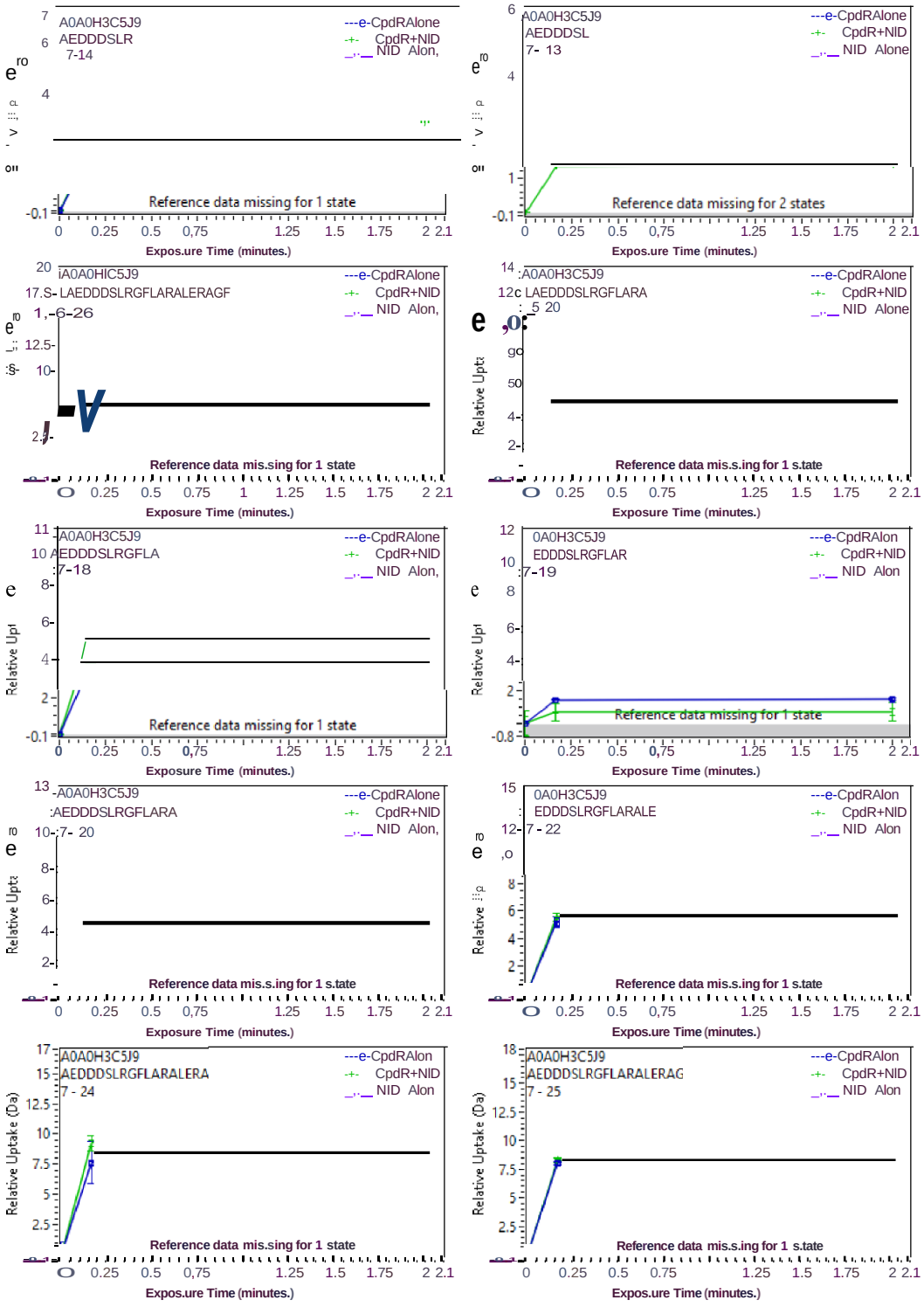
A0A0H3C5J9
AEDDDSLR
7-14
---e-CpdRAlone
-+- CpdR+NID
NID Alon,
Reference data missing for 1 state
Expos.ure Time (minutes.)
A0A0H3C5J9
AEDDDSL
7- 13
---e-CpdRAlone
-+- CpdR+NID
NID Alone
Reference data missing for 2 states
Expos.ure Time (minutes.)
iA0A0HIC5J9
17.S- LAEDDDSLRGFLARALERAGF
1,-6-26
---e-CpdRAlone
-+- CpdR+NID
NID Alon,
Reference data mis.sing for 1 state
Exposure Time (minutes.)
:A0A0H3C5J9
12c LAEDDDSLRGFLARA
: 5 20
---e-CpdRAlone
-+- CpdR+NID
NID Alone
Reference data mis.s.ing for 1 s.tate
Exposure Time (minutes.)
A0A0H3C5J9
AEDDDSLRGFLA
:7-18
---e-CpdRAlone
-+- CpdR+NID
NID Alon,
Reference data missing for 1 state
Exposure Time (minutes.)
0A0H3C5J9
EDDDSLRGFLAR
:7-19
---e-CpdRAlon
-+- CpdR+NID
NID Alon
Reference data missing for 1 state
Exposure Time (minutes.)
-A0A0H3C5J9
:AEDDDSLRGFLARA
:7- 20
---e-CpdRAlone
-+- CpdR+NID
NID Alon,
Reference data mis.s.ing for 1 s.tate
Exposure Time (minutes.)
0A0H3C5J9
EDDDSLRGFLARALE
7 - 22
---e-CpdRAlon
-+- CpdR+NID
NID Alon
Reference data mis.s.ing for 1 s.tate
Exposure Time (minutes.)
A0A0H3C5J9
AEDDDSLRGFLARALERA
7 - 24
---e-CpdRAlon
-+- CpdR+NID
NID Alon
Relative Uptake (Da)
Reference data mis.sing for 1 state
Expos.ure Time (minutes.)
A0A0H3C5J9
AEDDDSLRGFLARALERAG
7 - 25
---e-CpdRAlon
-+- CpdR+NID
NID Alon
Relative Uptake (Da)
Reference data mis.s.ing for 1 s.tate
Expos.ure Time (minutes.)

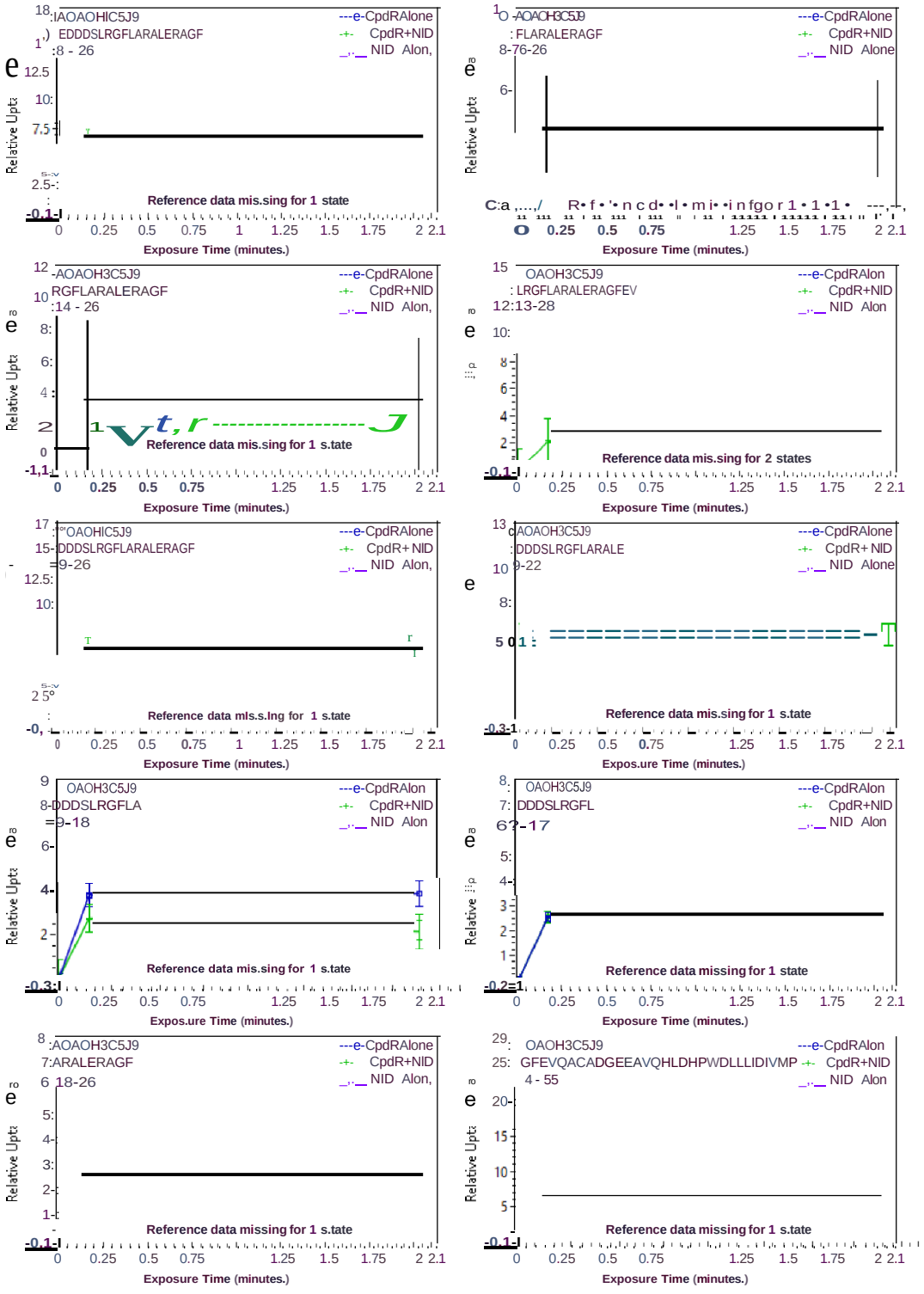
Relative Uptake
Exposure Time (minutes.)
Reference data mis.sing for 1 state
Reference data missing for 1 state
Reference data mis.sing for 2 states
Reference data mis.sing for 1 s.tate
Reference data missing for 1 s.tate
---e-CpdRAlone
CpdR+NID
NID Alone

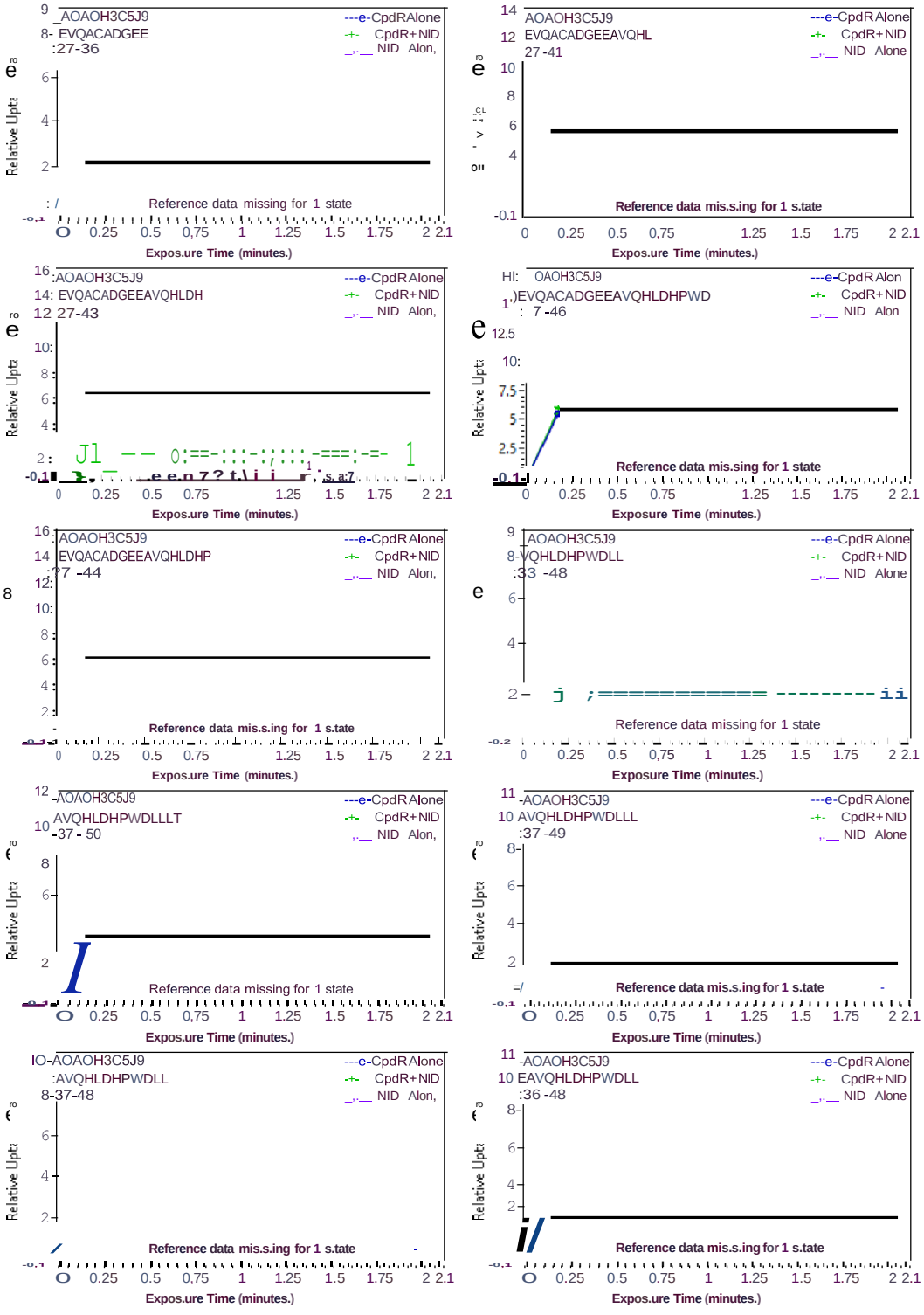
AOAOH3C5J9
EVQACADGEE
:27-36
---e-CpdRAlone
-+- CpdR+NID
NID Alon,
Relative Upta
Reference data missing for 1 state
Expos.ure Time (minutes.)
AOAOH3C5J9
EVQACADGEEAVQHL
27-41
---e-CpdRAlone
-+- CpdR+NID
NID Alone
Reference data mis.s.ing for 1 s.tate
Expos.ure Time (minutes.)
:AOAOH3C5J9
EVQACADGEEAVQHLDH
27-43
---e-CpdRAlone
-+- CpdR+NID
NID Alon,
Expos.ure Time (minutes.)
HI: OAOH3C5J9
EVQACADGEEAVQHLDHPWD
7-46
---e-CpdRAlon
-+- CpdR+NID
NID Alon
Reference data mis.sing for 1 state
Exposure Time (minutes.)
AOAOH3C5J9
EVQACADGEEAVQHLDHP
27-44
---e-CpdRAlone
-+- CpdR+NID
NID Alon,
Reference data mis.s.ing for 1 s.tate
Expos.ure Time (minutes.)
AOAOH3C5J9
VQHLDHPWDLL
:33-48
---e-CpdRAlone
-+- CpdR+NID
NID Alone
Reference data missing for 1 state
Exposure Time (minutes.)
-AOAOH3C5J9
AVQHLDHPWDLLLT
-37-50
---e-CpdRAlone
-+- CpdR+NID
NID Alon,
Reference data missing for 1 state
Expos.ure Time (minutes.)
-AOAOH3C5J9
AVQHLDHPWDLLL
:37-49
---e-CpdRAlone
-+- CpdR+NID
NID Alone
Reference data mis.s.ing for 1 s.tate
Expos.ure Time (minutes.)
IO-AOAOH3C5J9
:AVQHLDHPWDLL
8-37-48
---e-CpdRAlone
-+- CpdR+NID
NID Alon,
Reference data mis.s.ing for 1 s.tate
Expos.ure Time (minutes.)
-AOAOH3C5J9
EAVQHLDHPWDLL
:36-48
---e-CpdRAlone
-+- CpdR+NID
NID Alone
Reference data mis.s.ing for 1 s.tate
Expos.ure Time (minutes.)

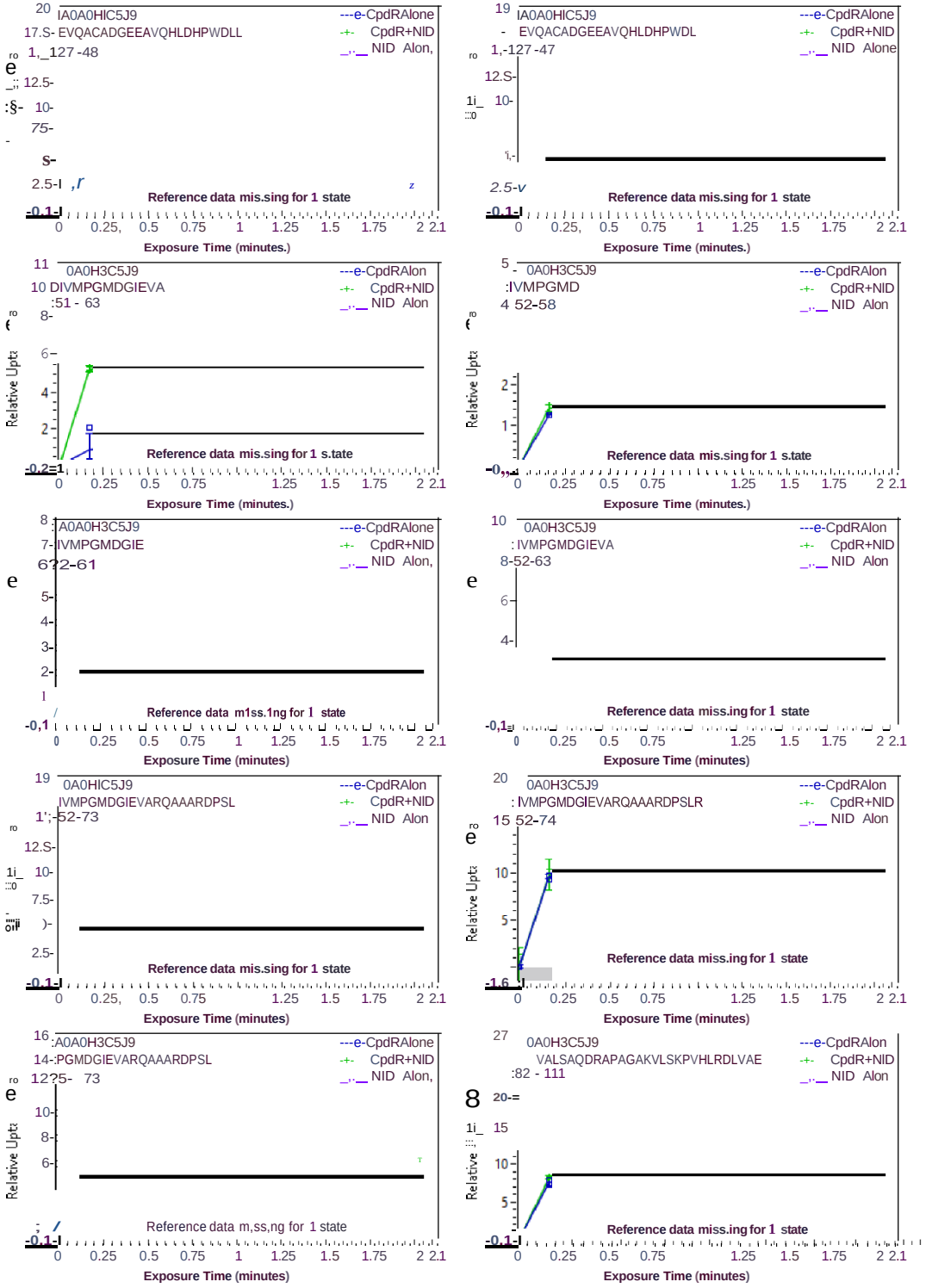
IA0A0HIC5J9
EVQACADGEEAVQHLDHPWDLL
---e-CpdRAlone
CpdR+NID
NID Alon,
Reference data mis.sing for 1 state
Exposure Time (minutes.)
IA0A0HIC5J9
EVQACADGEEAVQHLDHPWDL
---e-CpdRAlone
CpdR+NID
NID Alone
Reference data mis.sing for 1 state
Exposure Time (minutes.)
0A0H3C5J9
DIVMPGMDGIEVA
:51 - 63
---e-CpdRAlon
CpdR+NID
NID Alon
Relative Uptx
Reference data mis.sing for 1 s.tate
Exposure Time (minutes.)
0A0H3C5J9
:IVMPGMD
4 52-58
---e-CpdRAlon
CpdR+NID
NID Alon
Relative Uptx
Reference data mis.sing for 1 s.tate
Exposure Time (minutes.)
:A0A0H3C5J9
IVMPGMDGIE
---e-CpdRAlone
CpdR+NID
NID Alon,
Reference data m1ss.1ng for 1 state
Exposure Time (minutes)
0A0H3C5J9
: IVMPGMDGIEVA
8-52-63
---e-CpdRAlon
CpdR+NID
NID Alon
Reference data miss.ing for 1 state
Exposure Time (minutes)
0A0HIC5J9
IVMPGMDGIEVARQAAARDPSL
---e-CpdRAlon
CpdR+NID
NID Alon
Reference data mis.sing for 1 state
Exposure Time (minutes)
0A0H3C5J9
: IVMPGMDGIEVARQAAARDPSLR
15 52-74
---e-CpdRAlon
CpdR+NID
NID Alon
Relative Uptx
Reference data miss.ing for 1 state
Exposure Time (minutes)
:A0A0H3C5J9
14-:PGMDGIEVARQAAARDPSL
---e-CpdRAlone
CpdR+NID
NID Alon,
Relative Uptx
Reference data m,ss,ng for 1 state
Exposure Time (minutes)
0A0H3C5J9
VALSAQDRAPAGAKVLSKPVHLRDLVAE
:82 - 111
---e-CpdRAlon
CpdR+NID
NID Alon
Relative Uptx
Reference data miss.ing for 1 state
Exposure Time (minutes)

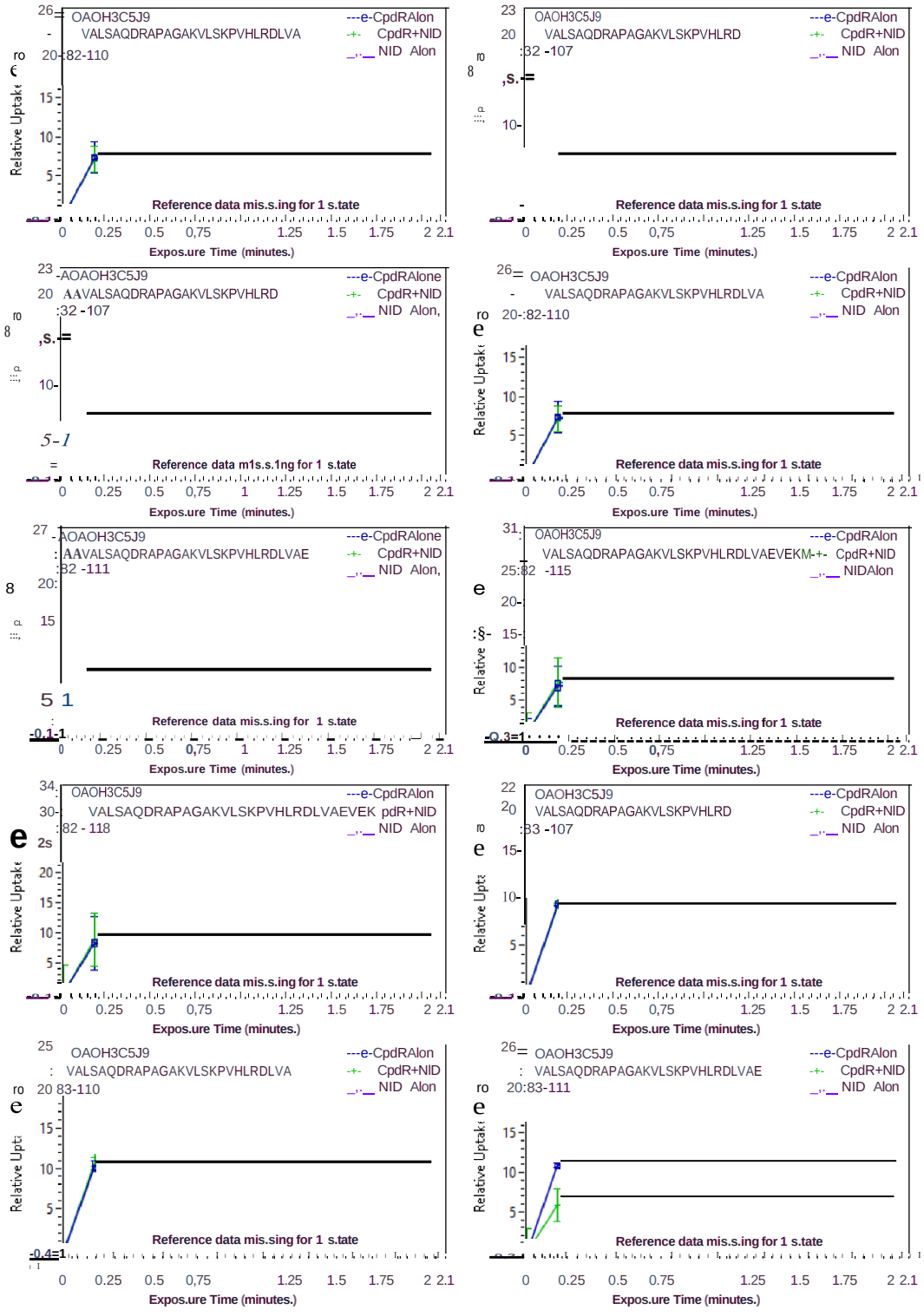
OAOH3C5J9
VALSAQDRAPAGAKVLSKPVHLRDLVA
20-82-110
---e-CpdRAlon
CpdR+NID
NID Alon
Relative Uptak
Reference data mis.s.ing for 1 s.tate
Expos.ure Time (minutes.)
OAOH3C5J9
VALSAQDRAPAGAKVLSKPVHLRD
:32 -107
---e-CpdRAlon
CpdR+NID
NID Alon
Reference data mis.s.ing for 1 s.tate
Expos.ure Time (minutes.)
-AOAOH3C5J9
AAVALSAQDRAPAGAKVLSKPVHLRD
:32 -107
---e-CpdRAlone
CpdR+NID
NID Alon,
Reference data m1s.s.1ng for 1 s.tate
Expos.ure Time (minutes.)
OAOH3C5J9
VALSAQDRAPAGAKVLSKPVHLRDLVA
20-:82-110
---e-CpdRAlon
CpdR+NID
NID Alon
Relative Uptak
Reference data mis.s.ing for 1 s.tate
Expos.ure Time (minutes.)
-AOAOH3C5J9
AAVALSAQDRAPAGAKVLSKPVHLRDLVAE
:82 -111
---e-CpdRAlone
CpdR+NID
NID Alon,
Reference data mis.s.ing for 1 s.tate
Expos.ure Time (minutes.)
OAOH3C5J9
VALSAQDRAPAGAKVLSKPVHLRDLVAEVEKM
25:82 -115
---e-CpdRAlon
CpdR+NID
NIDAlon
Relative
Reference data mis.s.ing for 1 s.tate
Expos.ure Time (minutes.)
OAOH3C5J9
VALSAQDRAPAGAKVLSKPVHLRDLVAEVEK pdR+NID
:82 - 118
---e-CpdRAlon
NID Alon
Relative Uptak
Reference data mis.s.ing for 1 s.tate
Expos.ure Time (minutes.)
OAOH3C5J9
VALSAQDRAPAGAKVLSKPVHLRD
:83 -107
---e-CpdRAlon
CpdR+NID
NID Alon
Relative Upt
Reference data mis.s.ing for 1 s.tate
Expos.ure Time (minutes.)
OAOH3C5J9
VALSAQDRAPAGAKVLSKPVHLRDLVA
20 83-110
---e-CpdRAlon
CpdR+NID
NID Alon
Relative Upt
Reference data mis.sing for 1 s.tate
Expos.ure Time (minutes.)
OAOH3C5J9
VALSAQDRAPAGAKVLSKPVHLRDLVAE
20:83-111
---e-CpdRAlon
CpdR+NID
NID Alon
Relative Uptak
Reference data mis.s.ing for 1 s.tate
Expos.ure Time (minutes.)

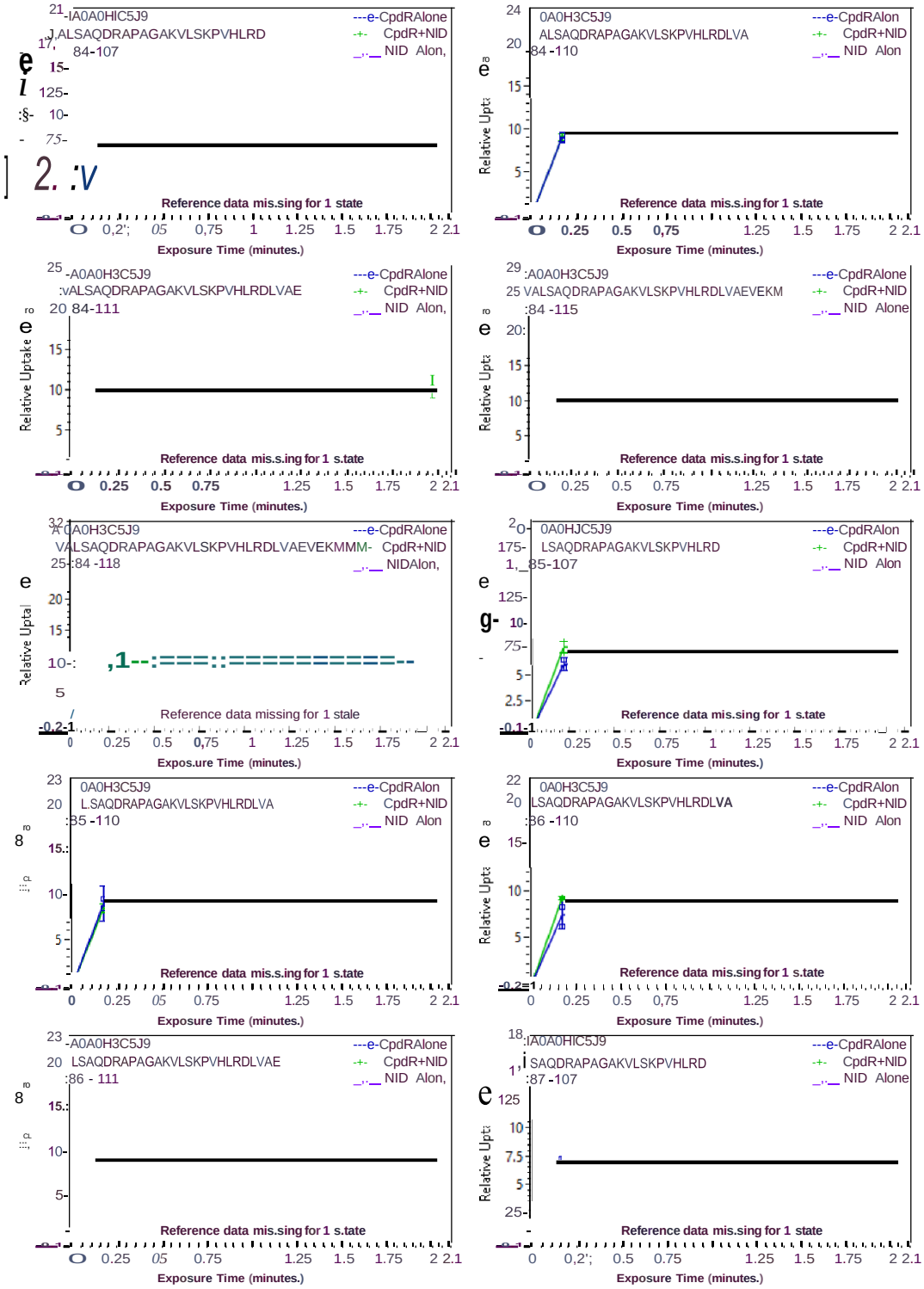
Reference data mis.s.ing for 1 s.tate
Exposure Time (minutes.)
Relative Uptake
Reference data missing for 1 stale
Expos.ure Time (minutes.)

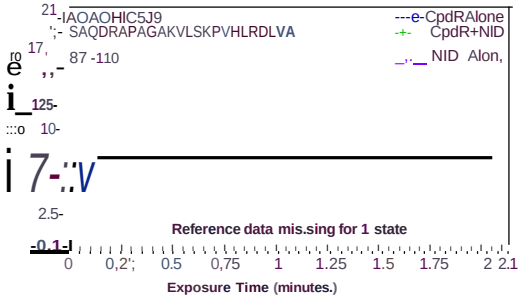
IAOAOHIC5J9
SAQDRAPAGAKVLSKPVHLRDLVA
87 -110
---e-CpdRAlone
CpdR+NID
NID Alon,
Reference data mis.sing for 1 state
Exposure Time (minutes.)

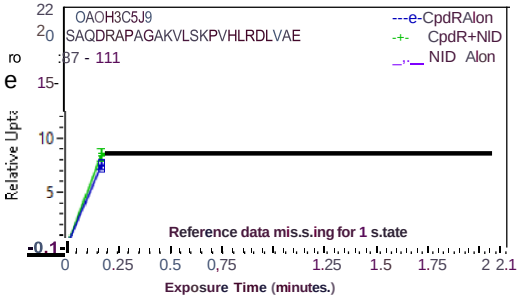
OAOH3C5J9
SAQDRAPAGAKVLSKPVHLRDLVAE
87 - 111
---e-CpdRAlon
CpdR+NID
NID Alon
Relative Upta
Reference data mis.s.ing for 1 s.tate
Exposure Time (minutes.)

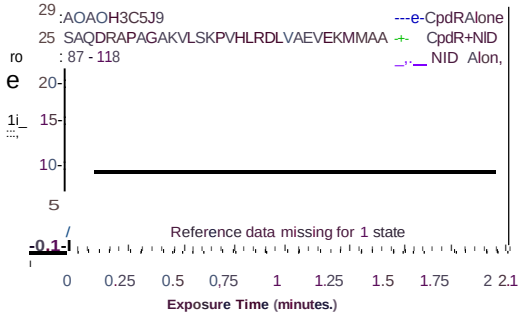
:AOAOH3C5J9
SAQDRAPAGAKVLSKPVHLRDLVAEVEKMMAA
87 - 118
---e-CpdRAlone
CpdR+NID
NID Alon,
Reference data missing for 1 state
Exposure Time (minutes.)

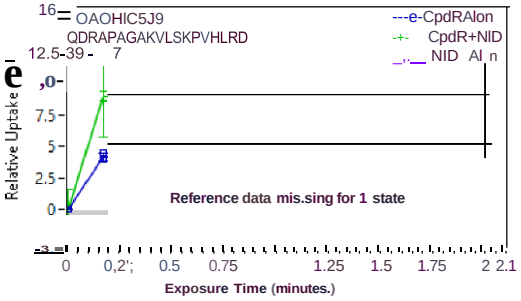
OAOHIC5J9
QDRAPAGAKVLSKPVHLRD
---e-CpdRAlon
CpdR+NID
NID Al n
Relative Uptake
Reference data mis.sing for 1 state
Exposure Time (minutes.)

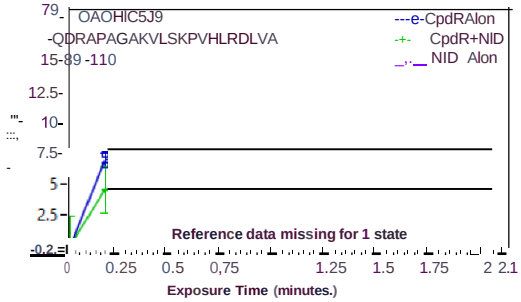
OAOHIC5J9
-QDRAPAGAKVLSKPVHLRDLVA
15-89 -110
---e-CpdRAlon
CpdR+NID
NID Alon
Reference data missing for 1 state
Exposure Time (minutes.)

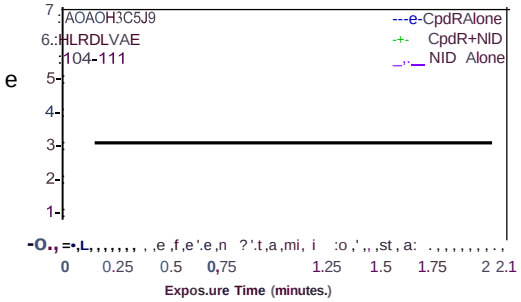
:AOAOH3C5J9
HLRDLVAE
104-111
---e-CpdRAlone
CpdR+NID
NID Alone
Expos.ure Time (minutes.)

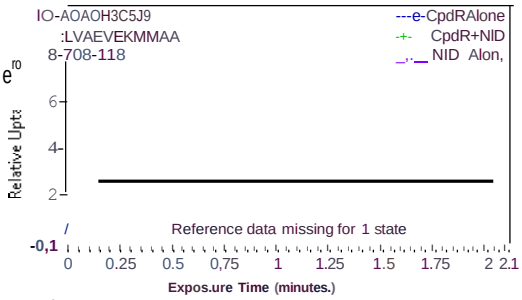
IO-AOAOH3C5J9
LVAEVEKMMAA
8-708-118
---e-CpdRAlone
CpdR+NID
NID Alon,
Relative Upta
Reference data missing for 1 state
Expos.ure Time (minutes.)

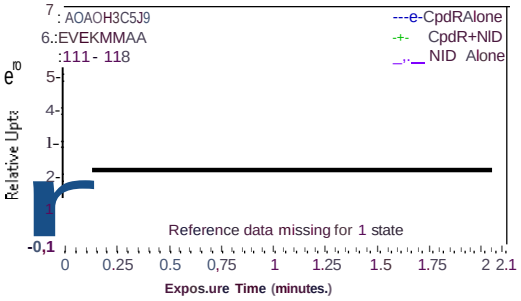
AOAOH3C5J9
EVEKMMAA
111 - 118
---e-CpdRAlone
CpdR+NID
NID Alone
Relative Upta
Reference data missing for 1 state
Expos.ure Time (minutes.)

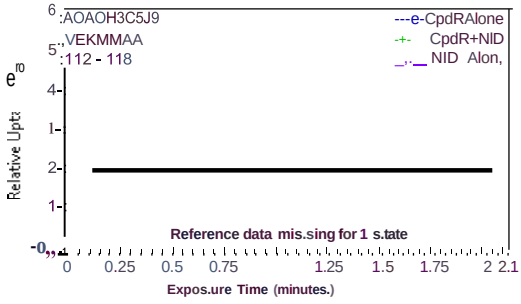
:AOAOH3C5J9
VEKMMAA
112 - 118
---e-CpdRAlone
CpdR+NID
NID Alon,
Relative Upta
Reference data mis.sing for 1 s.tate
Expos.ure Time (minutes.)

NTD ClpX Spectral Uptake Plots

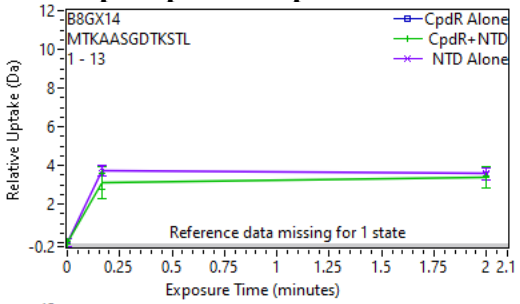

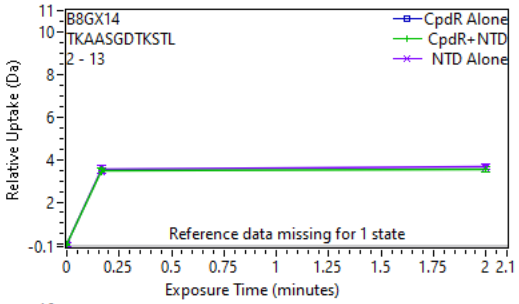

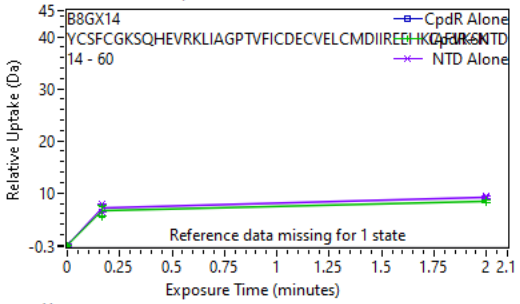

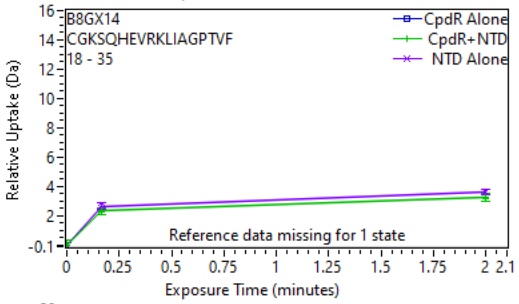

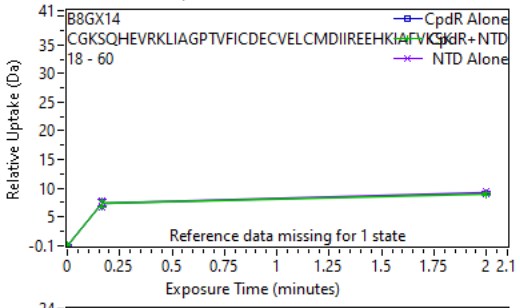

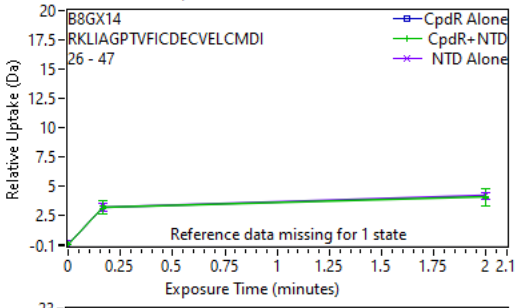

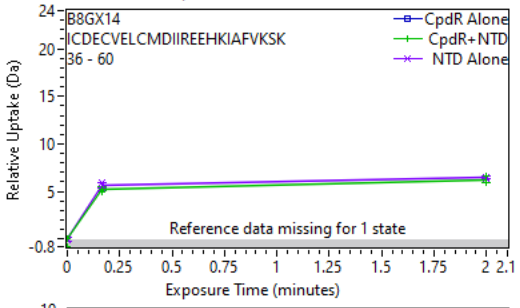

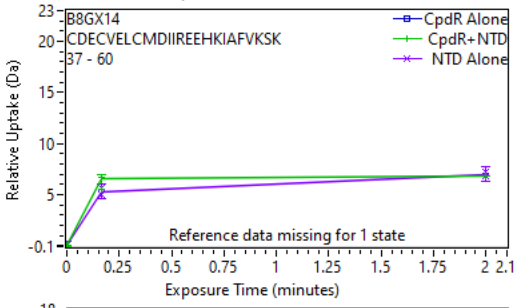

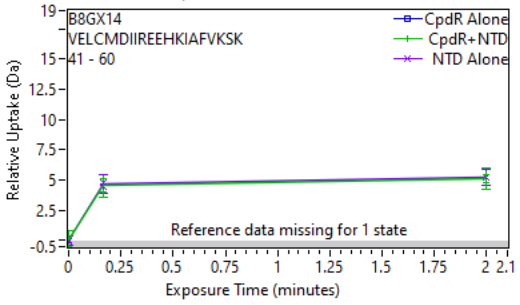

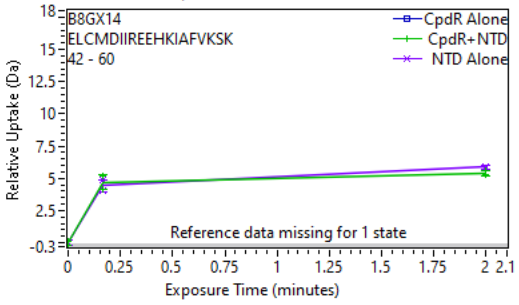

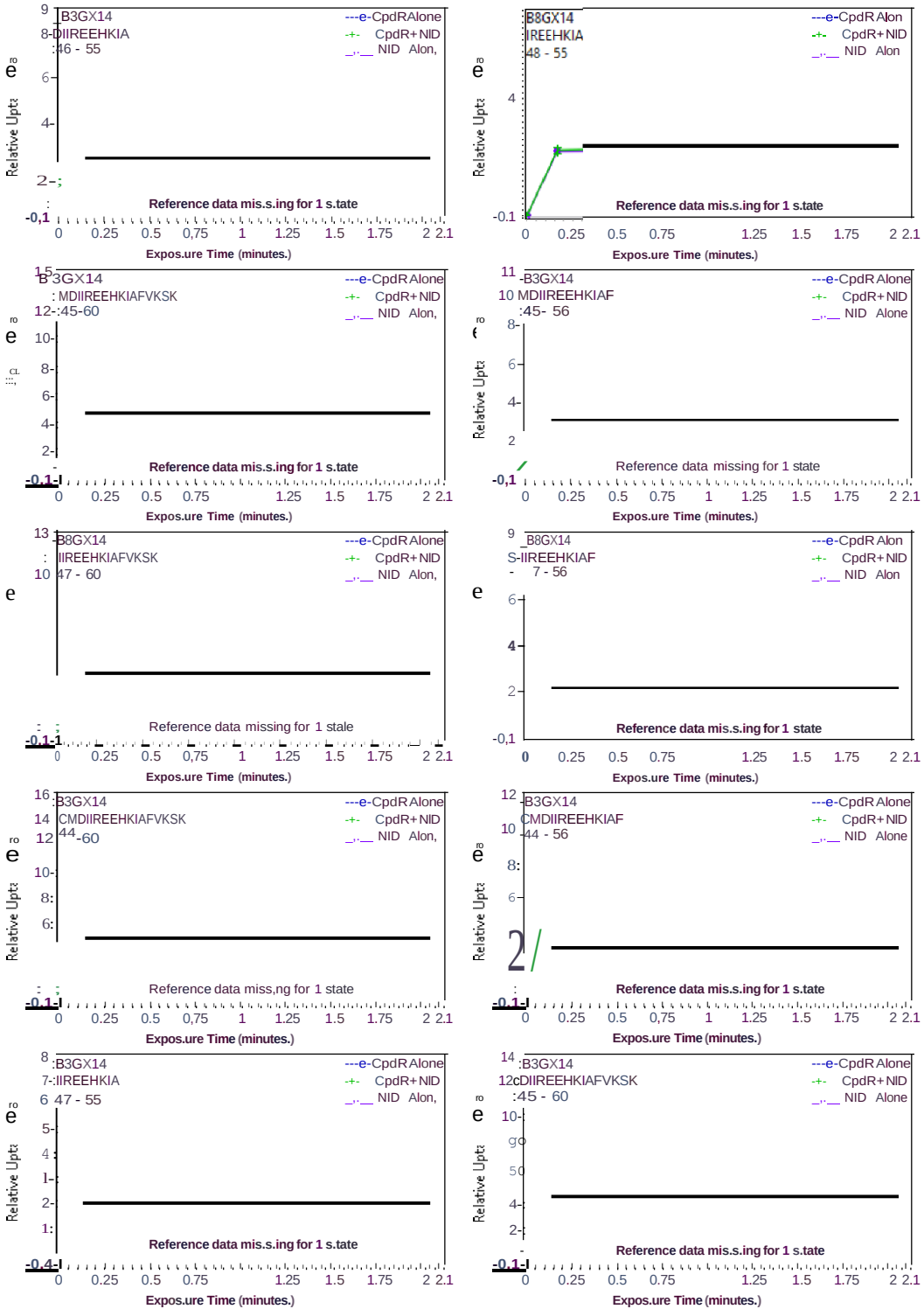
B3GX14
DIIREEHKIA
:46 - 55
---e-CpdRAlone
-+- CpdR+NID
_.-.__ NID Alon,
Relative Upta
Reference data mis.s.ing for 1 s.tate
Expos.ure Time (minutes.)
B8GX14
IREEHKIA
48 - 55
---e-CpdR Alon
-+- CpdR+NID
_.-.__ NID Alon
Reference data mis.s.ing for 1 s.tate
Expos.ure Time (minutes.)
B3GX14
: MDIIREEHKIAFVKSK
12-:45-60
---e-CpdR Alone
-+- CpdR+NID
_.-.__ NID Alon,
Reference data mis.s.ing for 1 s.tate
Expos.ure Time (minutes.)
-B3GX14
10 MDIIREEHKIAF
:45- 56
---e-CpdR Alone
-+- CpdR+NID
_.-.__ NID Alone
Reference data missing for 1 state
Expos.ure Time (minutes.)
B8GX14
: IIREEHKIAFVKSK
10 47 - 60
---e-CpdR Alone
-+- CpdR+NID
_.-.__ NID Alon,
Reference data missing for 1 stale
Expos.ure Time (minutes.)
_B8GX14
S-IIREEHKIAF
- 7 - 56
---e-CpdR Alon
-+- CpdR+NID
_.-.__ NID Alon
Reference data mis.s.ing for 1 state
Expos.ure Time (minutes.)
B3GX14
CMDIIREEHKIAFVKSK
44 -60
---e-CpdR Alone
-+- CpdR+NID
_.-.__ NID Alon,
Reference data miss,ng for 1 state
Expos.ure Time (minutes.)
B3GX14
CMDIIREEHKIAF
44 - 56
---e-CpdR Alone
-+- CpdR+NID
_.-.__ NID Alone
Reference data mis.s.ing for 1 s.tate
Expos.ure Time (minutes.)
:B3GX14
7-:IIREEHKIA
6 47 - 55
---e-CpdR Alone
-+- CpdR+NID
_.-.__ NID Alon,
Reference data mis.s.ing for 1 s.tate
Expos.ure Time (minutes.)
B3GX14
cDIIREEHKIAFVKSK
:45 - 60
---e-CpdR Alone
-+- CpdR+NID
_.-.__ NID Alone
Reference data mis.s.ing for 1 s.tate
Expos.ure Time (minutes.)

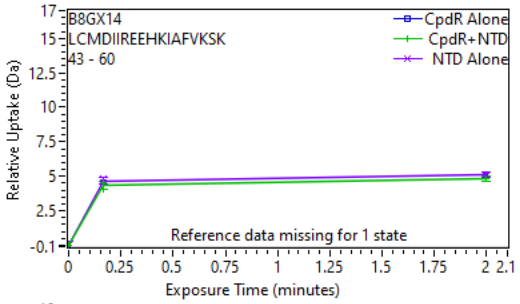
B8GX14
LCMDIIREEHKIAFVKSK
43 - 60
CpdR Alone
CpdR+NTD
NTD Alone
Relative Uptake (Da)
Reference data missing for 1 state
Exposure Time (minutes)

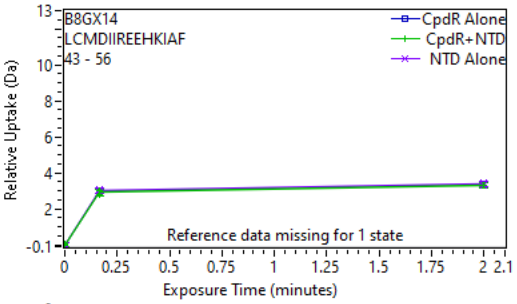
B8GX14
LCMDIIREEHKIAF
43 - 56
CpdR Alone
CpdR+NTD
NTD Alone
Relative Uptake (Da)
Reference data missing for 1 state
Exposure Time (minutes)

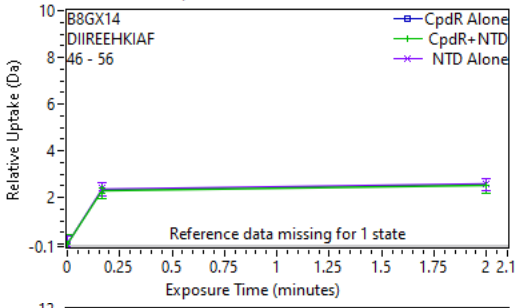
B8GX14
DIIREEHKIAF
46 - 56
CpdR Alone
CpdR+NTD
NTD Alone
Relative Uptake (Da)
Reference data missing for 1 state
Exposure Time (minutes)

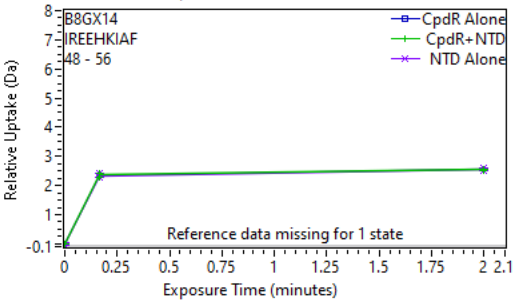
B8GX14
IREEHKIAF
48 - 56
CpdR Alone
CpdR+NTD
NTD Alone
Relative Uptake (Da)
Reference data missing for 1 state
Exposure Time (minutes)

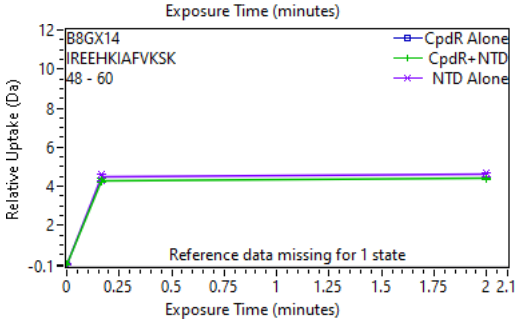
B8GX14
IREEHKIAFVKSK
48 - 60
CpdR Alone
CpdR+NTD
NTD Alone
Relative Uptake (Da)
Reference data missing for 1 state
Exposure Time (minutes)

REFERENCES

Iniesta, A.A., McGrath, P.T., Reisenauer, A., McAdams, H.H., and Shapiro, L. (2006). A phospho-signaling pathway controls the localization and activity of a protease complex critical for bacterial cell cycle progression. Proc. Natl. Acad. Sci. U.S.A. *103*, 10935–10940. 10.1073/pnas.0604554103.

Lau, J., Hernandez-Alicea, L., Vass, R.H., and Chien, P. (2015). A Phosphosignaling Adaptor Primes the AAA+ Protease ClpXP to Drive Cell Cycle-Regulated Proteolysis. Molecular Cell *59*, 104–116. 10.1016/j.molcel.2015.05.014.

Rood, K.L., Clark, N.E., Stoddard, P.R., Garman, S.C., and Chien, P. (2012). Adaptor Dependent Degradation of a Cell-Cycle Regulator Uses a Unique Substrate Architecture. Structure *20*, 1223–1232. 10.1016/j.str.2012.04.019.

Joshi, K.K., Bergé, M., Radhakrishnan, S.K., Viollier, P.H., and Chien, P. (2015). An Adaptor Hierarchy Regulates Proteolysis during a Bacterial Cell Cycle. Cell *163*, 419–431. 10.1016/j.cell.2015.09.030.

Blair, J.A., Xu, Q., Childers, W.S., Mathews, I.I., Kern, J.W., Eckart, M., Deacon, A.M., and Shapiro, L. (2013). Branched Signal Wiring of an Essential Bacterial Cell-Cycle Phosphotransfer Protein. Structure *21*, 1590–1601. 10.1016/j.str.2013.06.024.

Baker, T.A., and Sauer, R.T. (2012). ClpXP, an ATP-powered unfolding and protein-degradation machine. Biochimica et Biophysica Acta (BBA) - Molecular Cell Research *1823*, 15–28. 10.1016/j.bbamcr.2011.06.007.

Cooper GM. The Cell: A Molecular Approach. 2nd edition. Sunderland (MA): Sinauer Associates; 2000. Protein Degradation. Available from: https://www.ncbi.nlm.nih.gov/books/NBK9957/.

Chen, Y.E., Tsokos, C.G., Biondi, E.G., Perchuk, B.S., and Laub, M.T. (2009). Dynamics of Two Phosphorelays Controlling Cell Cycle Progression in *Caulobacter crescentus*. J Bacteriol *191*, 7417–7429. 10.1128/JB.00992-09.

Konermann, L., Pan, J., and Liu, Y.-H. (2011). Hydrogen exchange mass spectrometry for studying protein structure and dynamics. Chem. Soc. Rev. *40*, 1224–1234. 10.1039/C0CS00113A.

Bhat, N.H., Vass, R.H., Stoddard, P.R., Shin, D.K., and Chien, P. (2013). Identification of ClpP substrates in *Caulobacter crescentus* reveals a role for regulated proteolysis in bacterial development: *Caulobacter* ClpP substrates. Molecular Microbiology *88*, 1083–1092. 10.1111/mmi.12241.

Sauer, R.T., and Baker, T.A. (2011). AAA+ Proteases: ATP-Fueled Machines of Protein Destruction. Annu. Rev. Biochem. 80, 587–612.

Tania A. Baker, Robert T. Sauer, ClpXP, an ATP-powered unfolding and protein-degradation Machine, Biochimica et Biophysica Acta (BBA) - Molecular Cell Research,Volume 1823, Issue 1, 2012, Pages 15-28, ISSN 0167-4889, https://doi.org/10.1016/j.bbamcr.2011.06.007.

Olivares, A.O., Baker, T.A., and Sauer, R.T. (2016). Mechanistic insights into bacterial AAA+ proteases and protein-remodelling machines. Nat Rev Microbiol *14*, 33–44. 10.1038/nrmicro.2015.4.

Auld, D.S. (2001). [No title found]. BioMetals *14*, 271–313. 10.1023/A:1012976615056.

Bellsolell, L., Prieto, J., Serrano, L., and Coll, M. (1994). Magnesium Binding to the Bacterial Chemotaxis Protein CheY Results in Large Conformational Changes Involving its Functional Surface. J. Mol. Biol. *238*, 489–495.

Bourret, R.B. (2010). Receiver domain structure and function in response regulator proteins. Current Opinion in Microbiology *13*, 142–149. 10.1016/j.mib.2010.01.015.

Mahmoud, S.A., and Chien, P. (2018). Regulated Proteolysis in Bacteria. Annu. Rev. Biochem. *87*, 677–696. 10.1146/annurev-biochem-062917-012848.

Biondi, E.G., Reisinger, S.J., Skerker, J.M., Arif, M., Perchuk, B.S., Ryan, K.R., and Laub, M.T. (2006). Regulation of the bacterial cell cycle by an integrated genetic circuit. Nature *444*, 899–904. 10.1038/nature05321.

Abel, S., Chien, P., Wassmann, P., Schirmer, T., Kaever, V., Laub, M.T., Baker, T.A., and Jenal, U. (2011). Regulatory Cohesion of Cell Cycle and Cell Differentiation through Interlinked Phosphorylation and Second Messenger Networks. Molecular Cell *43*, 550–560. 10.1016/j.molcel.2011.07.018.

Donaldson, L.W., Wojtyra, U., and Houry, W.A. (2003). Solution Structure of the Dimeric Zinc Binding Domain of the Chaperone ClpX. Journal of Biological Chemistry *278*, 48991– 48996. 10.1074/jbc.M307826200.

Thibault, G., Yudin, J., Wong, P., Tsitrin, V., Sprangers, R., Zhao, R., and Houry, W.A. (2006). Specificity in substrate and cofactor recognition by the N-terminal domain of the chaperone ClpX. Proc. Natl. Acad. Sci. U.S.A. *103*, 17724–17729. 10.1073/pnas.0601505103.

Jenal, U. (2009). The role of proteolysis in the Caulobacter crescentus cell cycle and development. Research in Microbiology *160*, 687–695. 10.1016/j.resmic.2009.09.006.

Grishin, N.V. (2001). Treble clef finger--a functionally diverse zinc-binding structural motif. Nucleic Acids Research *29*, 1703–1714. 10.1093/nar/29.8.1703.

Mirdita, M., Schütze, K., Moriwaki, Y. *et al.* ColabFold: making protein folding accessible to all. *Nat Methods* **19**, 679–682 (2022). https://doi.org/10.1038/s41592-022-01488-1